NANO STRUCTURAL METAL COMPOSITES: SYNTHESIS, STRUCTURAL AND THERMAL CHARACTERIZATION

A THESIS SUBMITTED TO
THE GRADUATE SCHOOL OF NATURAL AND APPLIED SCIENCES
OF
MIDDLE EAST TECHNICAL UNIVERSITY

BY

KADİR KALELİ

IN PARTIAL FULFILLMENT OF THE REQUIREMENTS
FOR
THE DEGREE OF MASTER OF SCIENCE
IN
CHEMISTRY

JULY 2008

Approval of the thesis

NANO STRUCTURAL METAL COMPOSITES: SYNTHESIS, STRUCTURAL AND THERMAL CHARACTERIZATION

submitted by **KADİR KALELİ** in partial fulfillment of the requirements for the degree of **Master of Science in Chemistry Department**, **Middle East Technical University** by,

Prof. Dr. Canan Özgen
Dean, Graduate School of **Natural and Applied Sciences** _____

Prof. Dr. Ahmet M. Önal
Head of Department, **Chemistry** _____

Prof. Dr. H. Ceyhan Kayran
Supervisor, **Chemistry Dept., METU** _____

Prof. Dr. Jale Hacaloğlu
Co-Supervisor, **Chemistry Dept., METU** _____

Examining Committee Members:

Prof. Dr. Zuhal KÜÇÜKYAVUZ
Chemistry Dept., METU _____

Prof. Dr. H. Ceyhan KAYRAN
Chemistry Dept., METU _____

Prof. Dr. Jale HACALOĞLU
Chemistry Dept., METU _____

Assist. Prof. Dr. Ayşen YILMAZ
Chemistry Dept., METU _____

Assoc. Prof. Dr. Göknur BAYRAM
Chemical Engineering Dept., METU _____

Date: _____

I hereby declare that all information in this document has been obtained and presented in accordance with academic rules and ethical conduct. I also declare that, as required by these rules and conduct, I have fully cited and referenced all material and results that are not original to this work.

Name, Last Name : KADİR KALELİ

Signature :

ABSTRACT

NANO STRUCTURAL METAL COMPOSITES: SYNTHESIS,

STRUCTURAL AND THERMAL CHARACTERIZATION

Kaleli, Kadir

M.S., Department of Chemistry

Supervisor: Prof. Dr. Ceyhan Kayran

Co-Supervisor: Prof. Dr. Jale Hacaloğlu

July 2008, 63 pages

In this work , metal functional polymers, namely Cr-PS-b-P2VP, Co-PS-b-P2VP, Au-PS-b-P2VP, Fe-PS-b-P2VP and Mo-PS-b-P2VP were prepared by thermal reaction of hexacarbonylchromium, $Cr(CO)_6$, octacarbonyldicobalt,$Co_2(CO)_8$, hydrogentetrachloroaurate(III), $H(AuCl_4).4H_2O$, trichloroiron(III), $FeCl_3.6H_2O$, molybdenum(VI)oxide, MoO_3 and PS-b-P2VP. TEM images indicated formation of Au^{III}, Cr and Co nanoparticles. On the other hand, crystalline structures were detected for Fe-PS-b-P2VP and Mo-PS-b-P2VP. Samples involving nanoparticles were further characterized by FTIR, UV-Vis and direct pyrolysis mass spectroscopy techniques. FTIR analysis indicated dissapearance of characteristic carbonyl peaks of $Cr(CO)_6$ and $Co_2(CO)_8$ for Cr-PS-b-P2VP and Co-PS-b-P2VP samples. The appearance of a peak at about 467 cm^{-1} supported the formation of metal-nitrogen bond. Pyrolysis mass spectrometry analysis showed an increase in the thermal stability of P2VP chains involving coordinated pyridine units. The

thermal stability of these chains increased in the order Co< Cr <Au^{3+} indicating stronger coordination in the same order.

Keywords: Organometallic Polymer, Nano Structural Metal Composite, Pyrolysis

ÖZ

NANO YAPILI METALİK KOMPOZİTLER: SENTEZİ, YAPISAL VE ISIL KARAKTERİZASYONU

Kaleli, Kadir

Yüksek Lisans, Kimya Bölümü

Tez Yöneticisi: Prof. Dr. H. Ceyhan Kayran

Tez Yönetici Yardımcısı: Prof. Dr. Jale Hacaloğlu

Temmuz 2008, 63 sayfa

Bu çalışmada, hekzakarbonilkrom, $Cr(CO)_6$, oktakarbonildikobalt, $Co_2(CO)_8$, hidrojentetrakloroaltın(III), $H(AuCl_4).4H_2O$, triklorodemir(III), $FeCl_3.6H_2O$, molibden(VI)oksit, MoO_3 ve PS-b-P2VP'in ısıl tepkimesiyle Cr-PS-b-P2VP, Co-PS-b-P2VP, Au-PS-b-P2VP, Fe-PS-b-P2VP ve Mo-PS-b-P2VP adlı metal fonksiyonel polimerler hazırlanmıştır. TEM görüntüleri Au^{III}, Cr ve Co nano parçacıklarının oluştuğunu göstermiştir. Diğer yandan Fe-PS-b-P2VP ve Mo-PS-b-P2VP'in kristal yapıda olduğu tespit edilmiştir. Nano parçacık içeren örnekler ayrıca FTIR, UV-Vis ve direkt piroliz kütle spektroskopi teknikleri kullanılarak karakterize edilmiştir. FTIR analizi Cr-PS-b-P2VP ve Co-PS-b-P2VP örneklerindeki $Cr(CO)_6$ ve $Co_2(CO)_8$'e ait karakteristik karbonil piklerinin kaybolduğunu ve metal-azot bağının oluştuğunu destekleyen 467 cm^{-1} dolayında yeni bir pik ortaya çıktığını göstermiştir. Piroliz kütle spektrometre analizi koordine piridin birimleri içeren P2VP zincirlerinin ısıl dengelerindeki artışı

göstermiştir. Bu zincirlerin termal kararlılıkları Co< Cr <Au^{3+} sırasında artmaktadır. Bu da metal bağının gücünün de aynı sırayla arttığını göstermektedir.

Anahtar Kelimeler: Organometalik Polimer, Nano Yapılı Metal Kompozit, Piroliz

Dedicated to my family and my fiancée . . .

ACKNOWLEDGEMENTS

I would like to express my profound gratitude to my advisor, Prof. Dr. Ceyhan Kayran, and my co-advisor Prof. Dr. Jale Hacaloğlu for their guidance, support and patience during the course of this research as well as their unique imagination and great experience that I have benefited from. I wish to express my sincere appreciation to Mehmet Zahmakıran, Önder Metin and Yusuf Nur for their support and guidance to improve my skills during my study at Middle East Technical University.

I would like to thank Asst. Prof. Dr. Tamer Uyar (INANO/Denmark) for the TEM analysis in the thesis.

TUBITAK (106T656) is also gratefully acknowleged for the financial support.

I am obliged to each and every member of C-205 Laboratory, Aysegül Elmacı from Mass Spectrometry Laboratory for the great atmosphere in the laboratory and for friendship and finally of course every member of SCL for the great atmosphere in and out of the laboratory and for breakfast and lunch every weekday and etc…

I was extraordinarily fortunate in having such a wonderful mother, Nermin Kaleli, a father, Levent Kaleli and a brother, Gökay Kaleli. I could never have succeeded all of this without their support.

Words fail me to express my appreciation to my lovely fiancée Ceyda İhtiyar whose dedication, love and persistent confidence in me, has taken the load off my shoulder. I would also thank her family for accepting me as a member of the family, warmly.

TABLE OF CONTENTS

LIST OF TABLES

LIST OF FIGURES

FIGURES

LIST OF SCHEMES

CHAPTER 1

INTRODUCTION

Substances that are containing direct metal carbon bonds are known as organometallic compounds. The variety of the organic moiety in such compounds is practically infinite, ranging from alkyl substituents to alkenes, alkynes, carbonyls, and aromatic and heterocyclic compounds. Among these, metal carbonyl complexes have remained one of the most important classes of organometallic compounds with their unusual physical properties [1].

Transition metal-organic ligand complexes are the primary components of the backbones of main-chain organometallic polymers [2]. Great interest is being expressed in the production of the polymer composites containing inclusions of metals, the dimensions of which are comparable to those of macromolecules. Nanodimensional systems show unusual physicochemical properties much different from similar properties of substances found in blocklike or microheterogeneous states. In metal nanoparticles, variations occur in the parameters of the crystal lattice, in atomic dynamics, and in the thermal, electrical, and magnetic properties. These make nanocomposites to be used as selective and effective catalysts, and as sensors and selective membranes for devices with nonlinear optical features. Also, metal containing modifiers in the nanodispersed form are used to increase the refractoriness of polymeric materials and their resistance to thermooxidative aging and to improve the mechanical properties of them [3].

Two or more homogenous polymer fragments, joined together by covalent bonds to form more complex macromolecules are defined as block copolymers. Di-, tri-, or multiblock copolymers are linear and multiarm, starblock, or graft copolymers are nonlinear [4].

Block copolymers have the desirable feature that their morphology can be systematically controlled by varying the number of blocks, their lengths, and their chemical compositions [5]. Multiblock copolymers have been experimentally observed and theoretically predicted to assemble into well-defined morphologies [6]. Diblock copolymers can prefer different morphologies such as, cubic arrays of spheres, hexagonal arrays of cylinders, bicontinuous cubic phases, or lamellar, depending on the relative block lengths [5]. For example, for a diblock copolymer chain of constant volume, if the relative volume of one block is increased at the expense of the other, the preferred morphology tends to shift from lamellar arrangements to morphologies that have greater amounts of curvature at the block–block interface. A typical progression of morphologies from lamellar to gyroid to hexagonally arranged cylinders to cubically ordered spheres is illustrated in Figure 1.1 [6]. Triblock copolymers that are composed of three blocks can prefer even more complex structures, such as helical strands surrounding cylinders embedded in a continuous matrix [5].

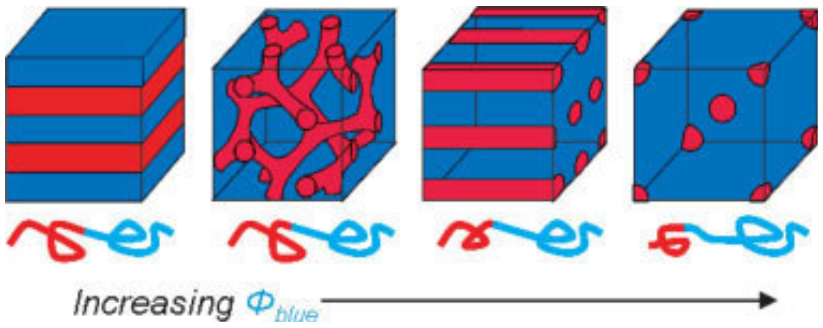

Figure 1.1. Influence of the Block Copolymer Composition as the Relative Volume Fraction (φ_{blue}) of One Block (blue) on the Bulk Morphology for a Constant Polymer Volume

Different methods can be applied for the preparation of metal functional polymers. Direct polymerization is one of these methods in which, the polymerization of metal-functional monomers leads to metal-containing copolymers [Scheme 1.1 (A)], which can often be further treated to afford polymer–nanoparticle composites by heating or using a reducing agent. [Scheme 1.1 (D)]. Metal functional polymers can also be prepared by direct assembly of polymers with nanoscale metallic species. Preformed polymers or copolymers are directly blended with metallic nanoparticles or nanoclusters [Scheme 1.1 (B)]. In this type, further structural control is enabled with the incorporation of specific interactions between polymers and nanoparticles, such as mutual hydrogen bonding moieties. Ligation of metals to ligand-functional polymers is another method used in the preparation of metal functional polymers. In this method, ligand-functional polymers are prepared either by the postpolymerization modification of appropriate precursor polymers or by the direct polymerization of ligand-functional monomers. To yield metal-functional polymers, they are treated with metal species either in solution or in bulk [Scheme 1.1 (C)], which may also be treated further to afford polymer–nanoparticle composites by heating or using a reducing agent. [Scheme 1.1 (D)] [6].

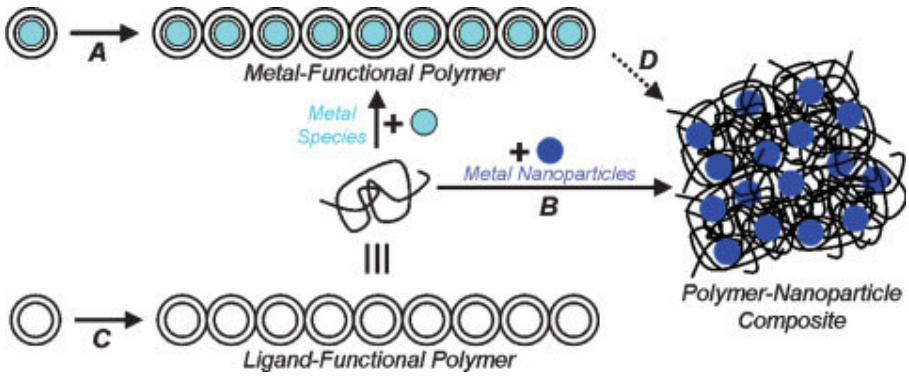

Scheme 1.1. Preparation of Metal-Polymer Composites

The synthesis of organometallic polymers by coordination of metals to plastics or other polymeric materials has gained significant interest as a consequence of their uses as conductors, liquid crystals, light emitting diodes and their interesting optical, magnetic and catalytic characteristics. On the other hand, the use of organometallic polymers for the preparation of nano structural metallic composites increases the importance of these materials even more. The literature work [6] indicates that the use of block copolymers, with interesting morphological characteristics in the synthesis of organometallic polymers yields several advantages in the preparation of nano structural metal composites. Though several studies on preparation and application of these important materials have been carried out, the knowledge of reaction mechanism and thermal characteristics that are very important for investigation of synthesis routes and application areas is still limited. Among several thermal analyses methods thermal gravimetry-FTIR (TG-FTIR), thermal gravimetry - mass spectrometry, (TG-MS), and pyrolysis mass spectrometry, (py-MS) are the ones that give information on not only thermal

stability but also on thermal degradation products. Among these the ones using mass spectrometer as a detector are more sensitive.

Pyrolysis is the chemical decomposition of a material in an inert atmosphere or in vacuum. It causes molecules to cleave at their weakest points to produce smaller, volatile fragments. Pyrolysis mass spectrometry (Py-MS) techniques can be regarded as most powerful analytical methods for thermal analysis of polymers. In these techniques, a pyrolysis system is coupled to a mass spectrometer to separate and identify pyrolysis products by ionizing, separating and measuring ions according to their mass-to- charge ratio (m/z). Pyrolysis mass spectrometry is an important technique in understanding structure and thermal behavior of polymers. Structural characterization of inorganic, organic, and bioorganic compounds can be achieved by using mass spectrometry technique [7,8]. There are two different types of pyrolysis-MS techniques; pyrolysis GC-MS and direct pyrolysis – MS, (DP-MS).

Although TGA-MS and pyrolysis GC-MS techniques are significantly sensitive, as only stable thermal degradation products can be detected, information on thermal decomposition mechanisms is limited. On the other hand, DP-MS technique offers several advantages. The high vacuum inside the mass spectrometer favors vaporization and thus allows the analysis of higher molecular mass pyrolyzates. Furthermore, as the high vacuum system rapidly removes the degradation products from the heating zone, secondary reactions and condensation reactions are avoided. In addition, the rapid detection system of the mass spectrometers allows detection of unstable thermal degradation products. Thus, thermal stability, degradation products and decomposition mechanism, which in turn can be used for structural characteristics of the compound under investigation, can be determined [9-14]. However, pyrolysis mass spectra of polymers are usually very complex, as thermal degradation products further dissociate in the mass spectrometer during ionization. Furthermore, all fragments with the same mass to charge ratio make contributions to the intensities of the same peaks in the mass spectrum. Thus, interpretation of the spectra is quite difficult. In this technique variation of total ion

yield as a function of temperature, the total ion current (TIC) curve is recorded in real time. Presence of more than one peak in the TIC curve indicates presence of either a multi-component sample or units with different thermal stabilities. On the other hand, scanning single ion current pyrograms allows separation of decomposition products as a function of volality and/or thermal stability. Thus, in case of direct pyrolysis MS analyses not only the detection of a peak, but also the variation of its intensity as a function of temperature, i.e. its evolution profile, is important. The trends in evolution profiles can be used to determine the source of the product, or the mechanism of thermal degradation.

Therefore, in this work, synthesis of organometallic polymers, nano structural metal composites and investigation of reaction mechanism and thermal characteristics have been aimed. Although the synthesis of organometallic polymers are known from literature [15-18], the use of pyrolysis mass spectrometry for the characterization of both block copolymer and the metal-polymers and also the formation of chromium nanoparticles using ligand functional polymer and organometallic complex have been performed for the first time in this thesis.

For this purpose, firstly, poly(styrene)-block-poly(vinyl-2-pyridine), (PS-b-P2VP), and octacarbonyldicobalt, $Co_2(CO)_8$, were chosen as target reactants. The thermal reaction of $Co_2(CO)_8$ with PS-b-P2VP leads to the formation of organometallic polymer in which copolymer coordinates to the metal through nitrogen atom of the pyridine ring (Fig 1.2) which then degrades to form nano particles. Later on, several organometallic polymers have been prepared by thermal reaction of trichloroiron(III), $FeCl_3.6H_2O$, molybdenum(VI)oxide, MoO_3, hexacarbonylchromium, $Cr(CO)_6$, hydrogentetrachloroaurate(III), $H(AuCl_4).4H_2O$, and PS-b-P2VP.

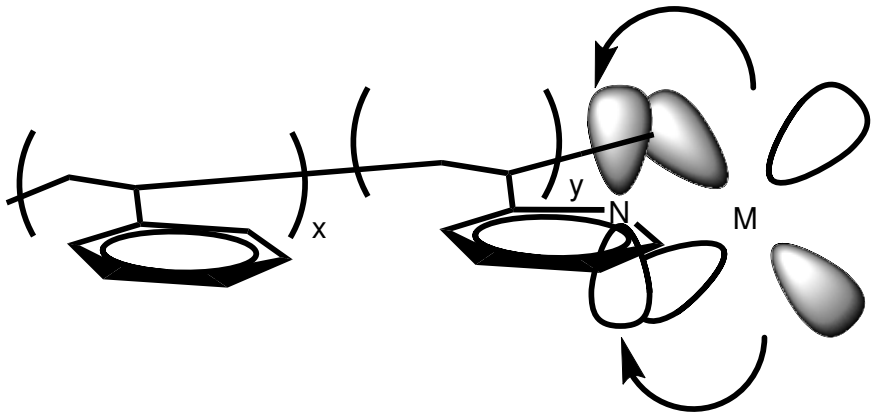

Figure.1.2. Coordination of PS-b-P2VP to the Transition Metal through Pyridine Nitrogen Atom

CHAPTER 2

BONDING

2.1. Metal Carbonyl Bonding

One of the most commonly encountered ligand in organo-transition metal chemistry is carbonmonoxide. It forms complexes with metals and these complexes are known as metal carbonyls. Its primary mode of attachment to metal atom is through the carbon atom [19].

The transiton metal CO bond can be described in the following resonance form;

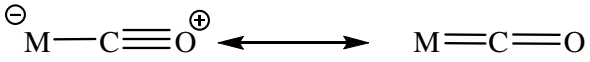

The bonding is more appropriately described in MO terms as following: The metal-carbon bond in metal carbonyl is believed to involve a σ-bond resulting from donation of the lone pair electron on carbon to the empty metal orbitals of σ-symmetry (Fig. 2.1a) and a π-bond due to the back donation of electrons from the filled dπ orbitals on the metals to the π-antibonding orbitals of carbonmonoxide (Fig. 2.1b) [20].

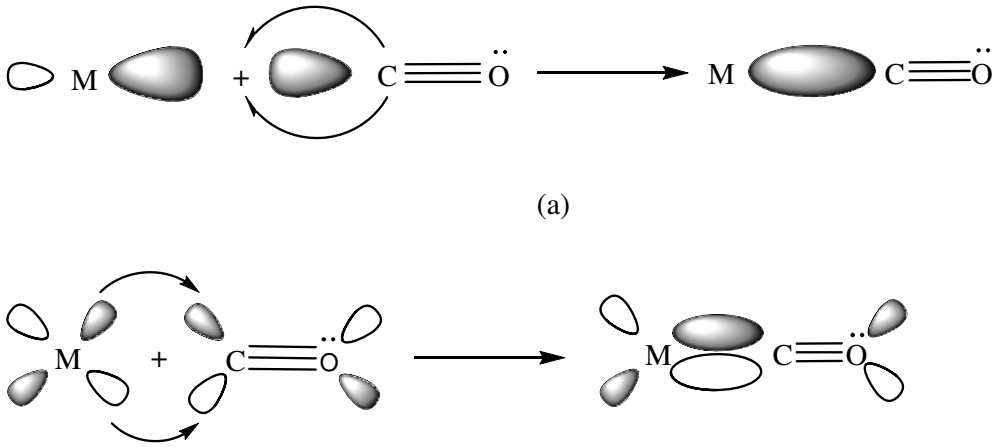

Figure 2.1. Molecular Orbital Description of Metal Carbonyl Interaction.

(a) The Formation of Carbon to Metal σ-bond, "σ-dative bond".

(b) The Formation of Metal to Carbon π-bond, "π-back bonding".

Basicity of CO increases as the back bonding makes the CO electron rich, which leads the drifting of electrons to the metal through the σ-bond. As a result of this, acidity and π-acceptor ability of CO increases, which causes the increasing of M-C bond strength and decreasing C-O bond strength.

The strength of the metal-carbonyl bonding and the extend of the π-bonding depends on the charge on the metal carbonyl or oxidation state of the metal. For instance, the negative charge on the metal atom places a large electron density on the central atom, which means, it will cause a strong metal-carbon π-bond due to the extent of electron donation to the carbon atom by the back donation, by this

way metal-carbon bonding will be shorter, while the carbon-oxygen bond becomes longer and weaker which directly effects the carbonyl stretching frequency.

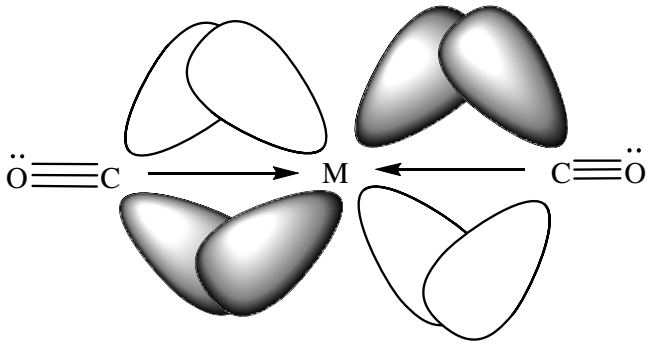

(a)

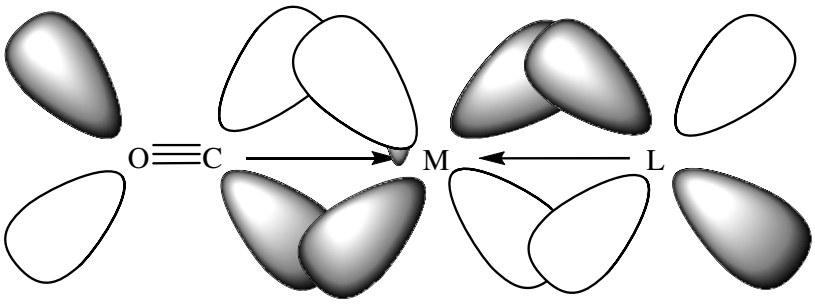

(b)

Figure 2.2. Competition for π-bonding in Metal Carbonyl Derivatives.

(a) Two equivalent ligands.

(b) Two different ligands with different π-accepting ability.

Not only carbonyl groups, but also other ligands have also an effect on the M-C and C-O bonds. Considering the two hypothetical molecules illustrated in Figure 2.2., in the OC-M-CO system both carbonyls compete equally for electron density from the metal, and so the π-bonds are equivalent. However, if L is a poor π-bonding ligand, it will not be able to compete successfully with the extremely good π-backbonding, ligand CO. Hence, the electron density will tend to drain off from the metal to the carbon monoxide, resulting a strong π-bond between M-C, and a weak one between M-L [21]. Consequently, the increase in the strength of the M-C bond weakens C-O bond and decreases carbonyl stretching frequency.

2.2. Metal Halide Bonding

The halides are known to be π donor ligand when coordinated to the metal, halides lone pairs are donated to the metal atom through π bonding (Fig. 2.3) and they are classified as weakly coordinating ligands but good leaving groups. As a result of this, when metal salts such as iron(III) chloride reacts with PS-b-P2VP, the halide ligand leaves the coordination sphere of the complex and PS-b-P2VP coordinates to the metal through pyridine nitrogen atom.

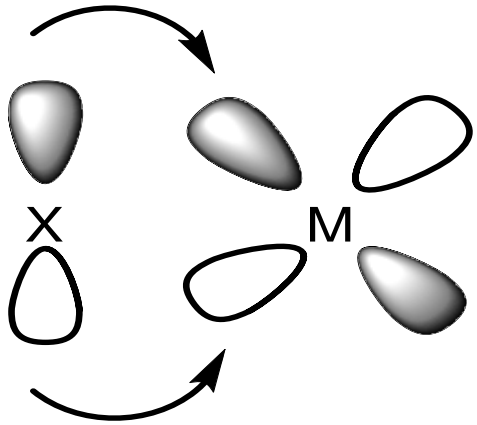

Figure 2.3. Metal Halide Bonding

2.3. Metal-Pyridine Bonding

Copolymer poly(styrene)-block-poly(2-vinylpyridine), Fig. 2.4 coordinates to the metal atom from its donor nitrogen atom. The nitrogen atom in pyridine is sp^2 hybrized. In the pyridine ring, the nitrogen sp^2 orbital containing only one electron overlaps with metal d orbital of σ symmetry (d_{x2-y2}) and donates electron to form a σ bond. On the other hand, the p orbital of nitrogen (containing one electron) perpendicular to the plane of the ring is capable of accepting an electron from metal d orbitals of (d_{xz} or d_{yz}) (Fig.2.5). As a conclusion, one can assume that the pyridine ligand is a σ- donor and π- acceptor ligand. The thermal reaction of the transition metal complexes with polystyrene-block-poly(2-vinylpyridine) proceeds through the coordination of pyridine nitrogen atom to the corresponding transition metal which then degradates to form nanoparticles**.**

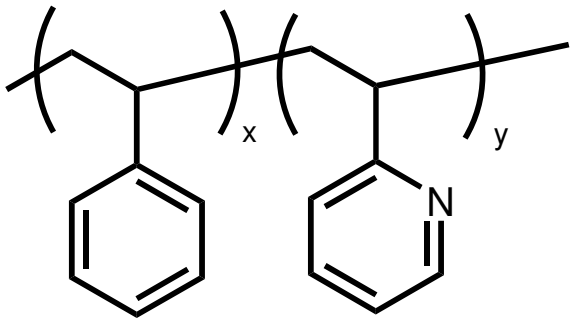

Figure 2.4. The Open Structure of Poly(styrene)-block-Poly(2-vinylpyridine)

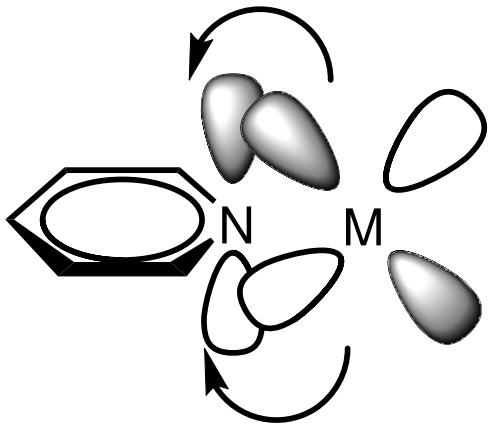

Figure 2.5. Metal-Pyridine Bonding Model

CHAPTER 3

EXPERIMENTAL

3.1. Basic Techniques

Most of the organometallic compounds are air sensitive and may decompose unless handled properly. Oxidation occurs at a significant rate at room temperature in many cases. Due to their sensitivity to oxygen and water, handling of organometallic compounds and all their reactions should be carried out under dry, deoxygenated nitrogen or argon atmosphere or under vacuum. Organometallic complexes may be handled almost as easily as ordinary compounds, if the reactions are carried out in the absence of oxygen, for example under dry and deoxygenated nitrogen gas atmosphere. For the preparation of deoxygenated nitrogen, nitrogen gas is allowed to pass through diphosphorus pentoxide (P_2O_5), then deoxygenated by using a catalyst and finally through dried molecular sieves to remove its moisture before using in the reaction medium. In general, the catalyst, copper(I)oxide should be heated to 120^{o}C using an electrical resistance, and hydrogen gas should be passed through the system from time to time to regenerate the catalyst (Fig.3.1).

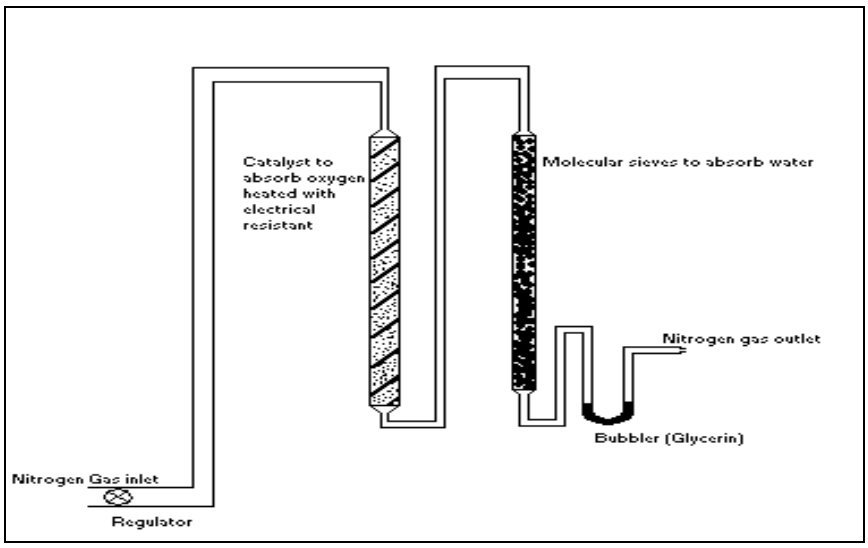

Figure 3.1. Nitrogen and Argon Gas Purification System.

The following techniques are generally employed for carrying out experiments with exclusion of oxygen,

(1) vacuum line technique is used to remove the solvent by evaporation in vacuum. Solvent is trapped in a tube immersed in liquid nitrogen.

(2) schlenk technique (Figure 3.2) in which a simple two-necked vessel, designed to permit passage of a nitrogen stream through the narrow neck with the stopcock while using the wider neck without a stopcock for operations such as inserting a spatula for scraping or removal of material, can be used. Depending on the objectives and the air sensitivity of the compounds, one technique or a combination of techniques is used.

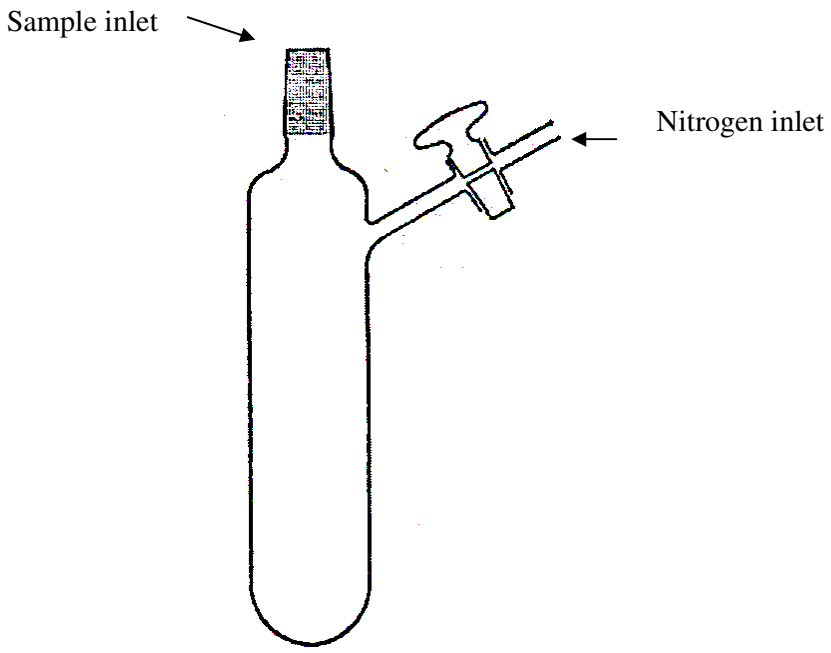

Figure 3.2 Standard Schlenk Tube

3.2. Chemicals

The transition metal complexes were purchased from Aldrich Chemical company and used without further purification. Polystyrene-block-poly2vinylpyridine was obtained from Beta chemical company having the polydispersity 1.03. (M_w= 76.735 kg/mole). Toluene, the only solvent used, purchased from Aldrich was purified by refluxing over metallic sodium under nitrogen for two or three days.

.

3.3. Synthesis of the Complexes

All the complexes were synthesized applying the same procedure known from literature with some modifications [22]. Table 3.1 lists the transition metal complexes and the products obtained by thermal reaction of metal complexes with polystyrene-block-poly(2-vinylpyridine). In this study, the thermal reaction between the transition metal complexes and PS-b-P2VP were performed by using two necked flask as shown in Fig. 3.3 with a nitrogen connection. All reactions were performed in a glow box under deoxygenated nitrogen atmosphere as $Co_2(CO)_8$ is very sensitive to oxygen and quickly decomposes. Actually, all the other transition metal complexes, namely $FeCl_3.6H_2O$, MoO_3, $Cr(CO)_6$ and $H(AuCl_4).4H_2O$ are not as sensitive as $Co_2(CO)_8$ to oxygen yet, all experiments were again performed in glow box to achieve identical experimental conditions. The deoxygenation of nitrogen was done using the system shown in Fig 3.1.

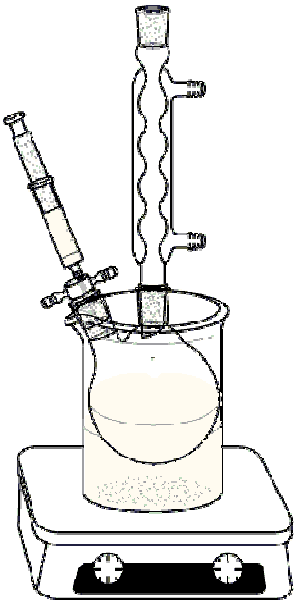

Figure. 3.3. The Apparatus Used During the Thermal Reaction.

Table 3.1. The Reactants Used During the Formation of Nanoparticles

Transition metal complexes	Product
Octacarbonyldicobalt, $Co_2(CO)_8$	cobalt -polystyrene-block-poly(2vinylpyridin) **Co-PS-b-P2VP**
Molybedenum(VI)oxide MoO_3	molybdenum-polystyrene-block-poly(2vinylpyridin) **Mo-PS-b-P2VP**
Iron(III)chloride, $FeCl_3.6H_2O$	iron - polystyrene- block-poly(2vinylpyridin) **Fe-PS-b-P2VP**
Hexacarbonylchromium $Cr(CO)_6$	chromium-polystyrene-block-poly(2vinylpyridin) **Cr-PS-b-P2VP**
Hydrogen tetrachloroaurate(III), $H(AuCl_4).4H_2O$	gold-polystyrene-block-poly(2vinylpyridin) **Au-PS-b-P2VP**

3.3.1. Synthesis of Cobalt Polystyrene-block-Poly2vinylpyridine (Co-PS-b-P2VP)

150 mg PS-b-P2VP was dissolved totally in 15 mL toluene (bp: 108-109^oC). To this solution, 300 mg (0.877 mmol) $Co_2(CO)_8$ was added. The mixture was refluxed under deoxygenated nitrogen atmosphere for 8 hours at the boiling point of toluene, at 110^oC. Finally, the solvent was evaporated under vacuum. The resultant product was analyzed by means of TEM, FTIR, UV-vis, and direct pyrolysis mass spectrometry techniques.

3.3.2. Synthesis of Chromium Polystyrene-block-Poly2vinylpyridine (Cr-PS-b-P2VP)

300 mg (1.363 mmol) $Cr(CO)_6$ was added to a solution prepared by dissolving 150 mg PS-b-P2VP in 15 mL toluene. The mixture was refluxed for 8 hours at 110^oC under nitrogen atmosphere. The color of the solution turned to dark violet indicating the coordination of metal to nitrogen. Finally, the solvent was evaporated under vacuum. The resultant product was analyzed by means of TEM, FTIR, UV-vis, and direct pyrolysis mass spectrometry techniques.

3.3.3. Synthesis of Gold Polystyrene-block-Poly2vinylpyridine (Au-PS-b-P2VP)

150 mg PS-b-P2VP was totally dissolved in 15 mL toluene. To this solution 300 mg (0.728 mmol) $H(AuCl_4).4H_2O$ was added. The mixture was refluxed for 8 hours at 110^oC under nitrogen atmosphere. Finally, the solvent was evaporated under vacuum. The resultant residue was analyzed by means of TEM, FTIR, UV-vis, and direct pyrolysis mass spectrometry techniques.

3.3.4. Synthesis of Iron Polystyrene-block-Poly2vinylpyridine (Fe-PS-b-P2VP)

300 mg (1.109 mmol) $FeCl_3.6H_2O$ was added to a solution prepared by dissolving 150 mg PS-b-P2VP in 15 mL toluene. After refluxing the mixture for 8 hours at 110^oC, the solvent was evaporated under vacuum and the resultant product was analyzed by means of TEM.

3.3.5. Synthesis of Molybdenum Polystyrene-block-Poly2vinylpyridine (Mo-PS-b-P2VP)

300 mg (2.084 mmol) MoO_3 was added to a solution prepared by dissolving 150 mg PS-b-P2VP in 15 mL toluene. Mixture was refluxed under nitrogen atmosphere for 8 hours at about 110^{o}C. As mentioned before, the solvent was evaporated under vacuum. The resultant product was analyzed by means of TEM.

3.4. Characterizations

3.4.1. Transmission Electron Microscope (TEM)

Transmission electron microscope (TEM) imaging of the nanoparticles was carried out with a Philips CM20 instrument at a 200kV. The nanoparticles were dispersed on the carbon-coated cupper grid from their diluted suspension of toluene. The synthesis of the metal nanoparticles were approved by TEM.

3.4.2. UV-Vis Spectra

The electronic absoption spectra of the samples were recorded on a Varian Cary 100 Bio UV-Vis Spectrophotometer with the concentrations about 1.2 x 10^{-5} M.

3.4.3. Infrared Spectra

FTIR analysis of the samples were performed by dropping a drop of samples on KBr pellet using Nicolet 510 FTIR Spectrometer.

3.4.4. Direct Pyrolysis Mass Spectrometry

Direct pyrolysis mass spectrometry (DPMS) system consisting a Waters Quattro Micro GC tandem mass spectrometer with an EI ion source and a mass range of 10-1500 Da was coupled a direct insertion probe (T_{max} = 650^{o}C). In each experiment, the temperature was kept constant at 50^{o}C for the first five minutes to remove any absorbed water and then increased to 650^{o}C at a heating rate of 10^{o}C/min, and kept constant for an additional 5 minutes at 650^{o}C. 0.010 mg samples were pyrolyzed in the quartz sample vials. Pyrolysis experiments were repeated at least twice to ensure reproducibility. 4200 mass spectra were obtained for each nano structural metal composite.

CHAPTER 4

RESULTS AND DISCUSSION

The characterization of the metal-functional polymers were first achieved by transmission electron microscope, TEM. For the samples involving metal nanostructures, characterizations were also performed by UV-visible, FTIR and direct pyrolysis mass spectrometry techniques.

4.1. Transmission Electron Microscope (TEM) Analysis

The TEM images of the five metal-functional polymers, Cr-PS-b-P2VP, Co-PS-b-P2VP, Au-PS-b-P2VP, Fe-PS-b-P2VP and Mo-PS-b-P2VP are shown in Fig. 4.1-4.5 respectively. As can be noticed from the figures, only chromium, cobalt and gold complexes formed nanoparticles when thermally reacted with PS-b-P2VP. Mo crystals can easily be differentiated. On the other hand the size of Cr and Co nanoparticles are comparable, while Au(III) nanoparticles are about more than 2-fold smaller (Table 4.1).

Table 4.1. Size of Nanoparticles

Name of Nanoparticle	Size of Nanoparticle (nm)
Chromium	20
Cobalt	20
Gold(III)	10

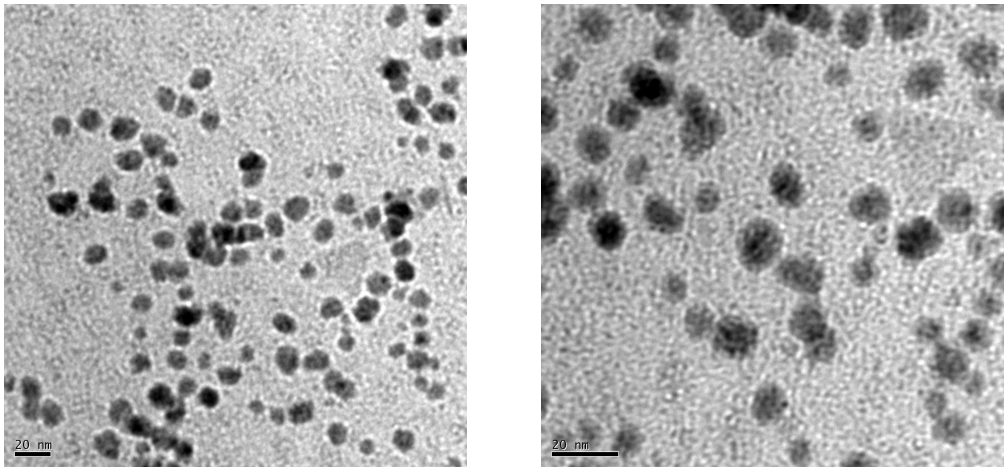

Figure 4.1. TEM Images of Cr-PS-b-P2VP

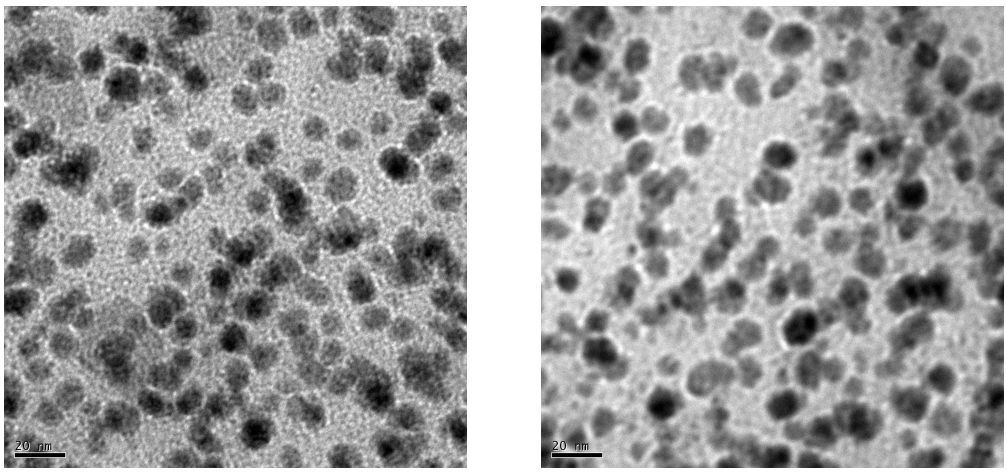

Figure 4.2. TEM Images of Co-PS-b-P2VP

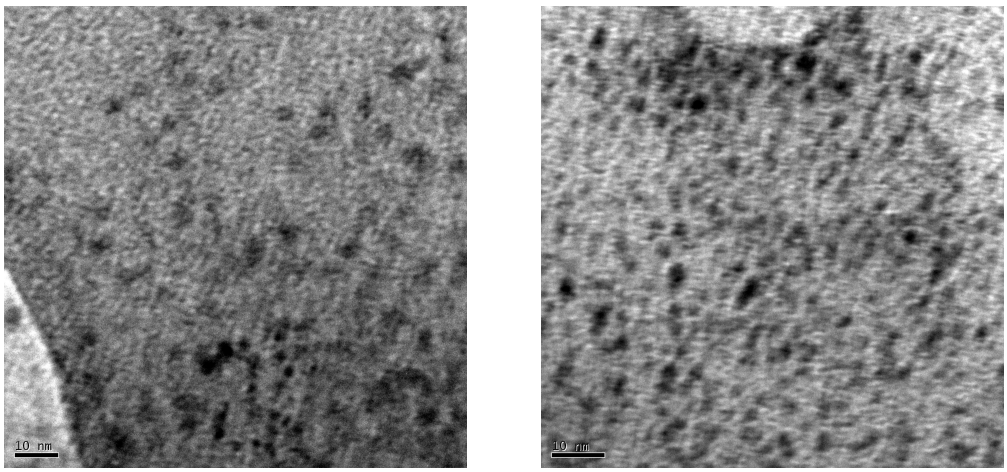

Figure 4.3. TEM Images of Au-PS-b-P2VP

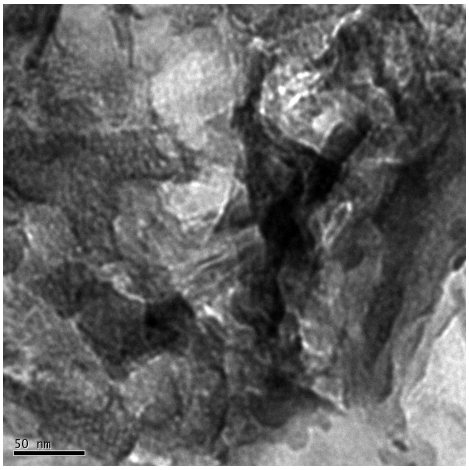

Figure 4.4. TEM Image of Fe-PS-b-P2VP

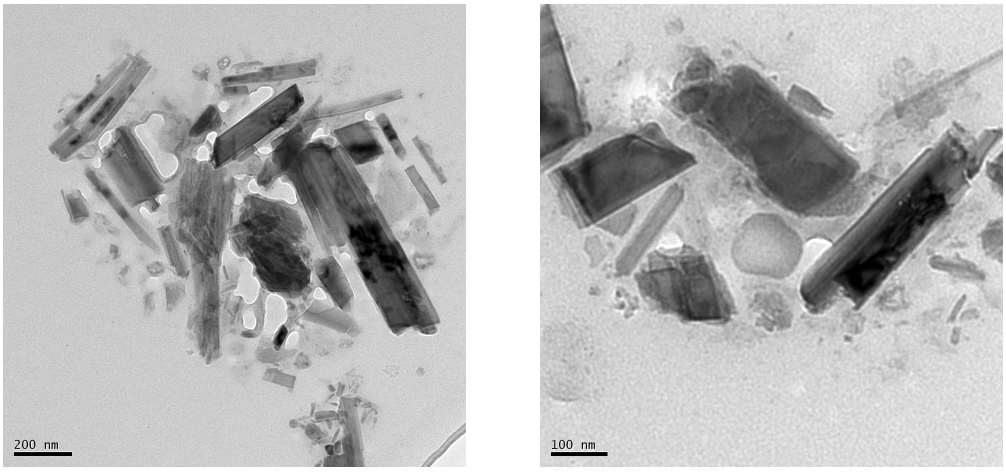

Figure 4.5. TEM Images of Mo-PS-b-P2VP

4.2 UV-Vis Characterization

4.2.1 Chromiumpolystyrene-block-poly(2-vinylpyridine)

Chromium nano particles are formed from the thermolysis of low spin $Cr(CO)_6$ complex with PS-b-P2VP. The UV-vis spectrum of the copolymer PS-b-P2VP shows an $\pi \rightarrow \pi^*$ transition band at around 295 nm due to pyridine and benzene ring. The starting organometallic complex $Cr(CO)_6$ involves an excellent π acceptor ligand, carbonyl, (having low lying π^*), thus, the UV-vis spectrum of the electron rich chromium atom shows a very strong absorption band at around 295-300 nm, due to metal to ligand charge transfer transition (MLCT).

In the UV-vis spectrum of the product Cr-PS-b-P2VP, the broad shoulder appeared at around 330 nm is attributed to a MLCT transition from chromium atom to π^* orbital of pyridine group. A weak absorption band is also observed at around 440 nm originating from ligand field transition (d-d transition) (Fig. 4.6).

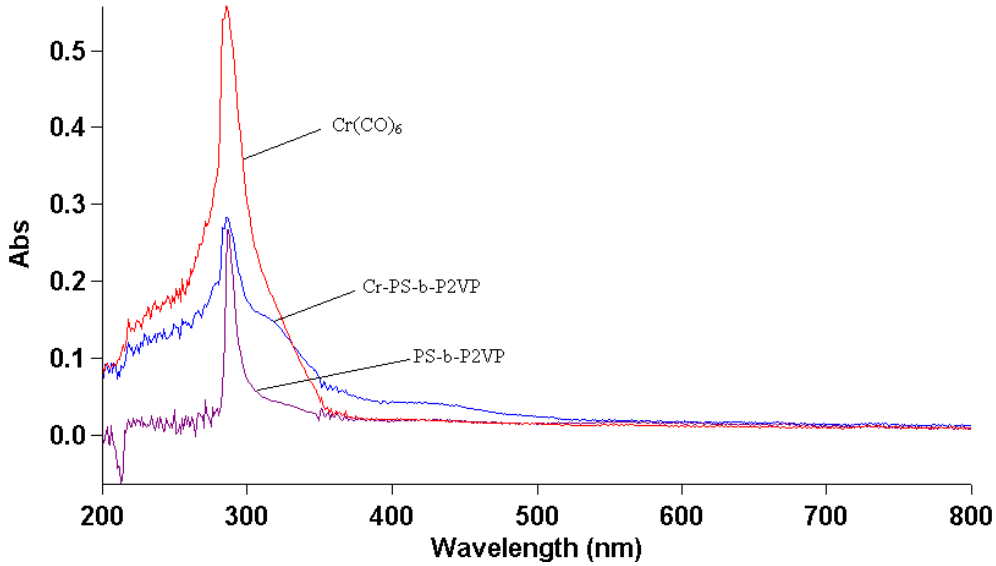

Figure 4.6. UV-Vis spectra of Cr-PS-b-P2VP, $Cr(CO)_6$, PS-b-P2VP

4.2.2 Cobaltpolystyrene-block-poly(2-vinylpyridine)

Cobalt nano particles are formed from the thermolysis of low spin $Co_2(CO)_8$ complex with PS-b-P2VP. $Co_2(CO)_8$ shows a very intense absorption peak at around 295 nm resulting from a MLCT transition from cobalt metal to π^* orbital of carbonyl group as observed in the case of chromium. For this complex, a broad middle intense band is also present as a shoulder at around 360 nm and may be associated with a spin forbidden MLCT transition.

The absorption spectrum of Co-PS-b-P2VP shows a very broad band. Some other absorptions bands arising from spin forbidden MLCT transitions and ligand field (LF) transition may be overlapped by this broad band (Fig. 4.7).

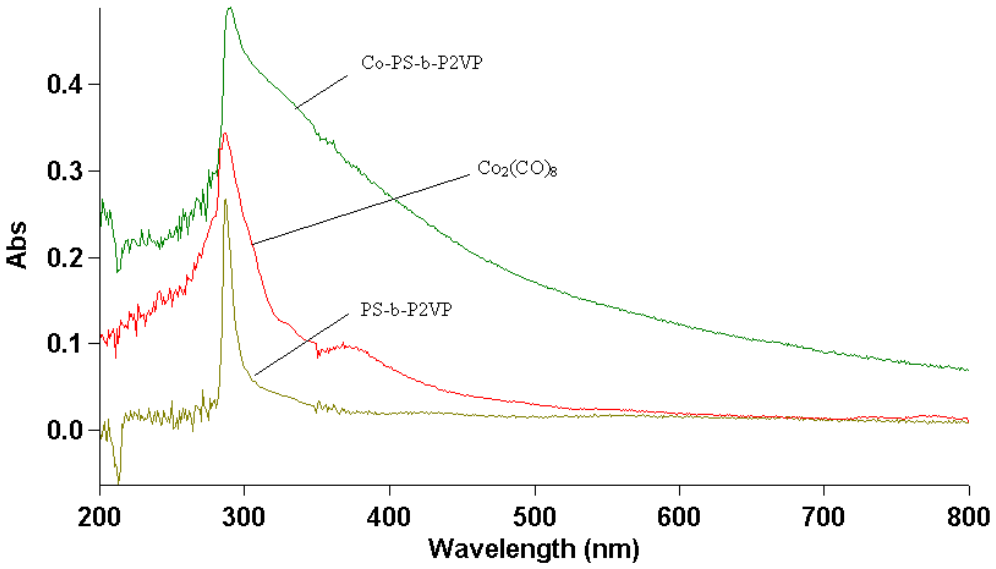

Figure 4.7. UV-Vis spectera of Co-PS-b-P2VP, $Co_2(CO)_8$ and PS-b-P2VP

4.2.3 Goldpolystyrene-block-poly(2-vinylpyridine)

Au(III) with its d^8 electronic configuration forms a variety of square-planar complexes. Since Au^{III} is an oxidizing agent, low-energy LMCT transitions are quite important. However, for this complex, MLCT transitions do not exist due to the lack of reducing properties of Au(III). As in the case of most of the electronic spectra of various halide compounds of gold [23-27], it is difficult to make complete assignments of absorption peaks due to the complications caused by the appearance of LMCT and less intense LF bands in the same energy range. UV-vis spectrum of the square planar tetrachloroaurate(III) complex exhibits LMCT transitions at around 295 nm. A broad shoulder appears at around 410 nm may be

attributed to spin forbidden LMCT transition. The less intense d-d transition may be under this broad LMCT band.

UV-vis spectrum of Au-PS-b-P2VP shows a completely new absorption band at around 320 nm which can be associated with a LMCT transition since gold is electron deficent and more willing to accept electrons from the ligand. When gold ion coordinates to pyridine nitrogen atom, nitrogen lone pair electrons are donated to the d orbitals of gold metal in order to overcome the electron deficency of the gold(III) ion (Fig.4.8).

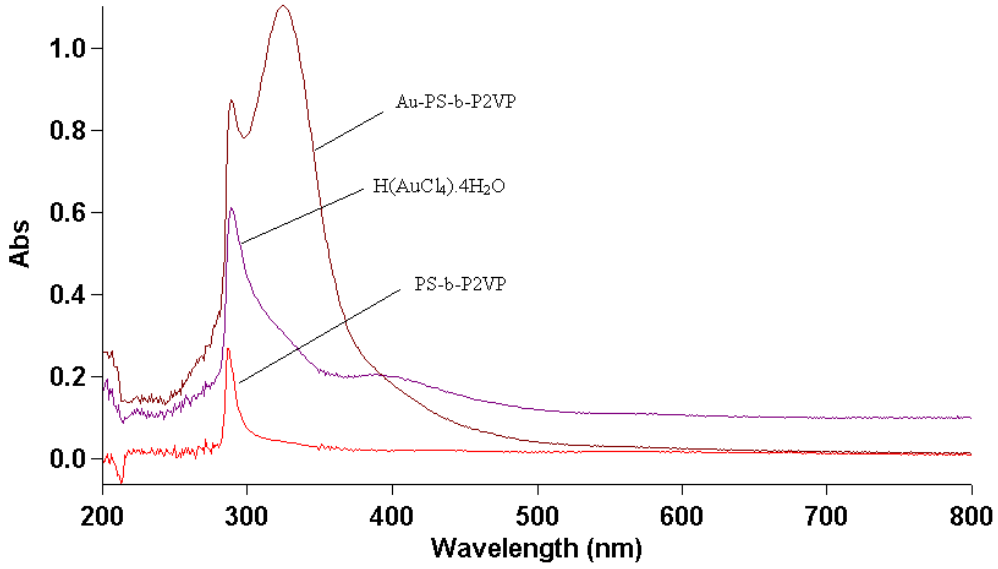

Figure 4.8. UV-Vis spectra of Au-PS-b-P2VP, $H(AuCl_4).4H_2O$ and PS-b-P2VP

4.3 FTIR Characterization

The formation of metal nanoparticles by reacting organometallic precursors in solutions of copolymer aggregates is known from literature [28-31]. It is known that aggregations were generated upon formation of metal nanoparticles by reactions of organometallic precursors with copolymers in solutions. These have included solutions of block copolymers [32,33] and surfactants [34]. In the literature studies, in all systems, the coordinating species consisted of pendent moieties that were polar than the solvent system employed for particle formation [35]**.** The hypothesis was that the metal precursors coordinates with an electron-rich segment of the copolymer (Fig. 1.2) and, upon heating the copolymers displace the precursor ligands (e.g. carbon monoxide, halides etc) to afford metal nanoparticles encased in copolymer sheath. It is reasoned that this could result from diffusion of the metal precursor into the core of a copolymer micelle where coordination and then reaction takes place. The same strategy was used in the present work. The organometallic precursors reacted thermally with PS-b-P2VP for 8 hours for the generation of metal nanoparticles. The nanoparticle formation starts by the coordination of the electron-rich segment of the copolymer that is 2-vinylpyridine, to the metal atom with the exclusion of the ligands. As a result, by the coordination of pyridine nitrogen to the metal atom or ion, the pyridine stretching and bending modes should be affected.

The FTIR spectrum of polystyrene-b-poly2-vinylpyridine (PS-b-P2VP), shows the characteristic absorption peaks of P2VP blocks at around 1594, 1472, 1431, 991, and 546 cm^{-1} for the C-H pyridine ring stretching mode and 750 cm^{-1} for the C-H pyridine bending mode. Polystyrene block of the copolymer gives absorption peaks at around 2500-3000 cm^{-1} due to C-H groups of phenyl ring. Several peaks in the range 1500-2500 cm^{-1} are assigned to C-C stretching modes of the aromatic rings, benzene and pyridine.

4.3.1 Chromiumpolystyrene-block-poly(2-vinylpyridine)

Actually, the most valuable information obtained from FTIR spectrum of Cr-PS-b-P2VP is the disappearence of the very intense absorption peak of carbonyl ligand of hexacarbonylchromium complex at around 2000 cm^{-1}. The metal vibrations have been observed in the range 500-200 cm^{-1} in the coordination complexes involving metal nitrogen bonds [36]. Thus, the new absorption peak appeared at around 464 cm^{-1} is attributed N-Cr stretching due to coordination of the pyridine nitrogen to the chromium metal. Significant changes were detected in the FTIR spectrum of Cr-PS-b-P2VP compared to that of the copolymer (Fig. 4.9). The relative intensities of the absorption peaks, in the range of 1590-600 cm^{-1}, especially, the ones at around 1594 cm^{-1} 1472 and 1431 cm^{-1} due to the pyridine strecthing and bending modes are decreased significantly. Furthermore, significant decreases in the intensity of the peaks present in 1500-2500 cm^{-1} range (where peaks due to C-C and C=C bond stretchings of the aromatic rings, both pyridine and styrene) are also detected upon coordination of the chromium metal to the pyridine nitrogen. On the other hand, the absorption peaks due to C-H stretching modes at around 2500-3000 cm^{-1} seemed to be not affected much.

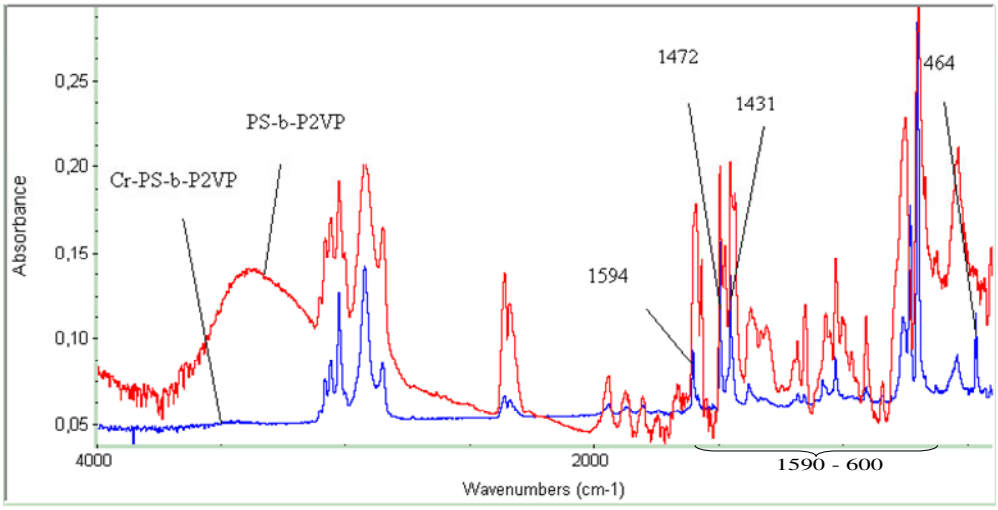

Figure 4.9. FTIR Spectra of PS-b-P2VP and Cr-PS-b-P2VP

4.3.2 Cobaltpolystyrene-block-poly(2-vinylpyridine)

The starting material, bimetallic cobalt complex has two types of carbonyl groups, namely, terminal and bridging. Having a C_2v symmetry, three absorption peaks for the terminal CO groups (ν_{CO} : 2023, 2041, 2071 cm^{-1}) and one absorption peak for the two collinear bridging carbonyl groups (ν_{CO}: 1847 cm^{-1}) are expected. (Fig.4.10). For the Co-PS-b-P2VP, the overlap of bridging carbonyl stretching peaks with characteristic polystyrene peaks is expected. Thus, in order to investigate the displacement of CO ligands by pyridines, the changes in the peaks associated with terminal carbonyl groups (2023, 2041, 2071 cm^{-1}) are analyzed. It can clearly be seen from Fig 4.10 that, the FTIR spectrum of the cobalt-functional polymer does not show any peak that can be attributed to absorption of terminal carbonyl groups confirming displacement of carbonyl groups completely. The new absorption peak appeared at around 467 cm^{-1} is again associated with N-metal

stretching mode as in case of Cr-PS-b-P2VP supporting the coordination of pyridine nitrogen to cobalt metal (Fig.4.11).

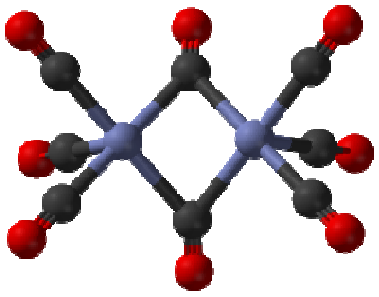

Figure 4.10. The Structure of $Co_2(CO)_8$

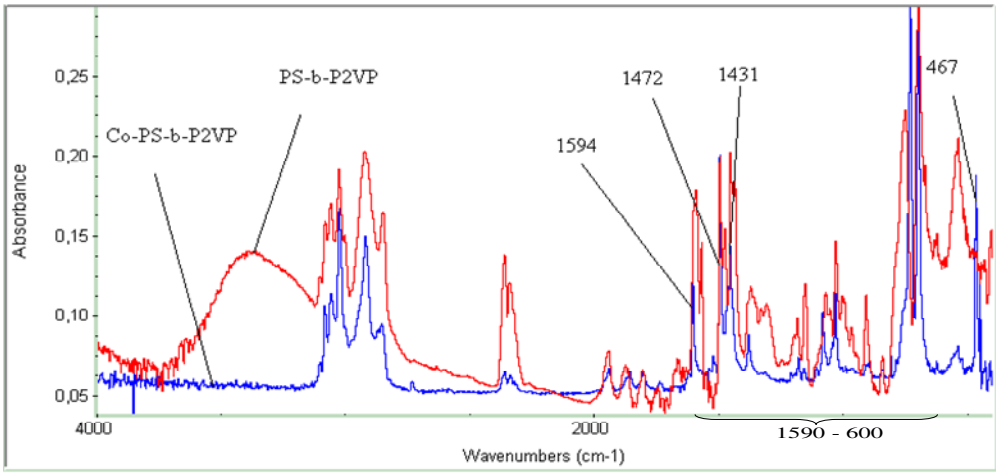

Figure 4.11. FTIR Spectra of PS-b-P2VP and Co-PS-b-P2VP

Similarly, the intensity of the absorption peaks in the range of 1590-600 cm^{-1} due to the pyridine stretching and bending modes drastically decrease as a result of the coordination of pyridine nitrogen to the cobalt metal.

4.3.3 Goldpolystyrene-block-poly(2-vinylpyridine)

The coordination of pyridine nitrogen to the gold(III) ion has been confirmed again by the changes in the intensities of the absorption peaks as in the cases of Cr-PS-b-P2VP and Co-PS-b-P2VP. Worthwhile changes are observed, especially in the range of 1590-600 cm^{-1}, where pyridine stretching and bending modes were observed, indicating the coordination of the pyridine nitrogen to the gold ion. As in the cases of Cr and Co samples mentioned before, the new absorption peak appeared at around 467 cm^{-1} supports the coordination of pyridine nitrogen to the gold ion but different from chromium and cobalt complexes, gold(III) ion is electron deficient and pyridine nitrogen donates its lone pair to the gold(III) ion through σ bonding (Fig. 4.12).

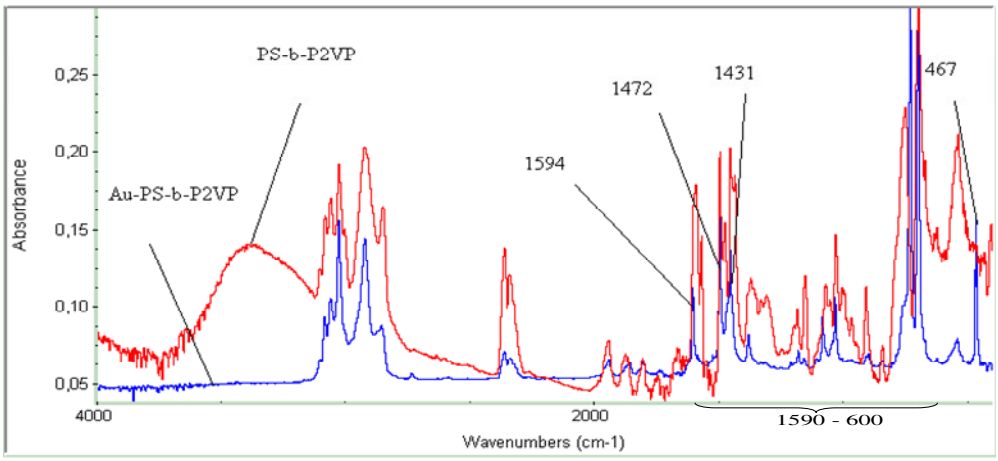

Figure 4.12. FTIR spectra of PS-b-P2VP and Au-PS-b-P2VP

4.4 Direct Pyrolysis Mass Spectrometry Characterization

As discussed before analysis of pyrolysis mass spectra of even homopolymers are quite complicated. In our case, as the samples under investigation, involving metals and block copolymers, having a quite complex structure should be expected to yield very complex pyrolysis mass spectra. Thus, in order to have a better understanding, pyrolysis mass spectra of the metal-functional copolymers were compared with those of the homopolymers, namely polystyrene and poly(2-vinylpyridine) and the copolymer, polystyrene-block-poly(2-vinylpyridine).

4.4.1 Polystyrene-block-poly(2-vinylpyridine)

Thermal decomposition of poly(2-vinyl pyridine) occurs by opposing reactions [37].

a. Depolymerization yielding mainly monomer

b. Loss of pyridine

c. Proton transfer to N atom yielding unsaturated linkages on the polymer backbone which in turn increases thermal stability.

It is known that the thermal degradation of PS takes place by a free-radical chain reaction, depolymerization, yielding mainly the styrene monomer and low molecular weight oligomers [38-41].

In Figure 4.13, total ion current (the variation of total ion yield as a function of temperature), (TIC) curve and the pyrolysis mass spectra at the peak maximum, at 427^{o}C and at the shoulder, at 393^{o}C, recorded during the pyrolysis of polystyrene-block-poly(2-vinylpyridine) are shown. A weak peak with maximum around 110^{o}C was also detected. Analyses of mass spectra indicated that the low temperature peak at 110^{o}C was due to evolution of the solvent, toluene adsorbed on the sample. Above 350^{o}C, generation of series of fragments such as $M_{x,}$ [M_x-CH_2], [M_x-CH], M_xCH, M_xCH_2, $M_xC{\equiv}CH$, $M_xCH{=}CH_2$ where M is either C_6H_5 or C_5H_4N and x =1, 2, 3, or 4 were observed. Peaks due to fragments stabilized by hydrogen exchange reactions were also detected [37]. In Table 4.2 the series of fragments detected and their m/z values are summarized.

Table 4.2. Series of Fragments Generated During the Pyrolysis of Polystyrene-block-Poly(2-vinylpyridine)

M / X	Styrene					2-vinyl pyridine			
	1	2	3	4		1	2	3	4
$M_{x,}$	104	208	312	416		105	210	315	420
$[M_x\text{-}CH_2]$		194	298	402			196	301	406
$[M_x\text{-}CH]$	91	193	297	401		92	195	300	405
M_xCH	117	221	325	429		118	223	328	433
M_xCH_2	118	222	326	430		119	224	329	434
$M_xC{\equiv}CH$	129	233	337	447		130	235	340	445
$M_xCH{=}CH_2$	131	235	339	443		132	237	342	447

For the copolymer, the base peak was at m/z=91 Da due to C_7H_7, and the most intense peaks were due to styrene (St) and vinylpyridine (VP) monomers and low mass oligomers in accordance with the literature results [37]. The relative intensities and the assignments made for the intense and characteristic peaks detected during the pyrolysis of the copolymer are collected in Table 4.3.

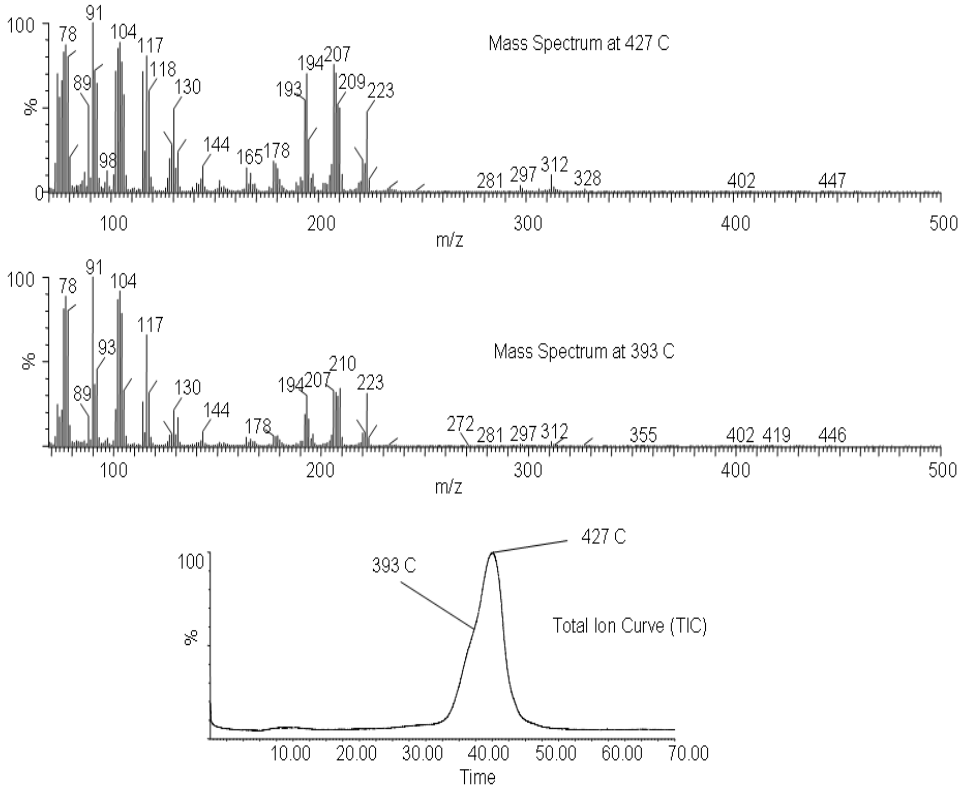

Figure 4.13. The TIC Curve and the Pyrolysis Mass Spectra Recorded at Peak Maximum and at the Shoulder for PS-b-P2VP

In Figure 4.14, the single ion evolution profiles of some selected products namely St (C_8H_8) and [VP-H], $(C_6H_5)CH\text{-}CH{=}CH_2$ and $(C_5H_4N)CH{=}C{=}CH_2$, [$St_2 - CH_2$], [St_2 – H], St dimer, St trimer, St tetramer, StH and VP, VP dimer, $VP_2(CH)$ and St_2CH_3, VP trimer, VP tetramer are shown.

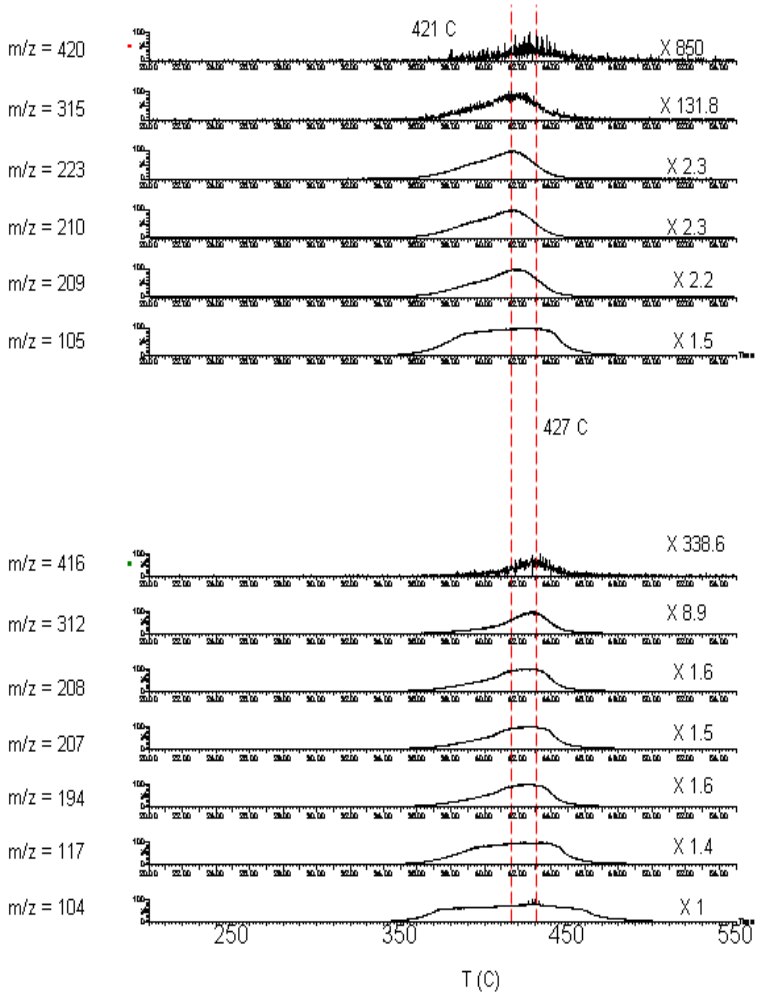

Figure 4.14. Single Ion Evolution Profiles of Some Selected Characteristic Products of PS-b-P2VP

Pyrolysis mass spectrometry data showed that both of the components degraded independently. Thermal stability of poly(2-vinyl pyridine) blocks were lower than that of polystyrene blocks. The yields of thermal degradation products of P2VP and PS were maximized at around 418, and 427°C respectively. Evolution profiles

of protonated oligomers of P2VP showed maxima at slightly higher temperatures compared to corresponding oligomers, around 421°C.

Table 4.3. Relative Intensities and the Assignments for the Intense and/or Characteristic Peaks in the Pyrolysis Mass Spectra of PS-b-P2VP Recorded at the Given Temperatures.

m/z	418°C	427°C	PS-b-P2VP Assignment
91	1000	1000	C_7H_7, C_6H_5N
92	693	673	C_7H_8, C_6NH_6
104	882	848	St, C_8H_8, [VP-H]
105	764	727	StH, VP
116	223	272	$(C_6H_5)CH=C=CH_2$,
117	790	746	$(C_6H_5)CH-CH=CH_2$, $(C_5H_4N)CH=C=CH_2$
118	587	539	$(C_5H_4N)CH-CH=CH_2$, $StCH_2$
129	249	334	$StC\equiv CH$
130	477	460	$PVC\equiv CH$
165	136	154	$C_{13}H_8$,
178	166	201	$C_{15}H_{11}$
179	155	187	$C_{15}H_{12}$
194	687	702	$[St_2 - CH_2]$
195	296	261	$[St_2 - CH]$, $[VP_2 - CH_3]$
207	739	729	$[St_2 - H]$
208	689	679	St dimer
209	518	411	St_2H, $[VP_2 - H]$
210	517	335	VP dimer
211	98	75	VP_2H
221	175	182	$St(C_6H_5)CH-CH=CH_2$, $VP(C_5H_4N)C=C=CH_2$
223	6.2	325	$VP_2(CH)$ St_2CH_3
312	94	122	St trimer
315	7.3	6.7	VP trimer
316	6.9	6.9	VP_3H
416	2.4	1.8	St tetramer,
419	0.7	0.4	$[VP_4 - H]$
420	0.6	0.4	VP tetramer

4.4.2. Chromiumpolystyrene-block-poly(2-vinylpyridine)

In Figure 4.15, the TIC curve and the pyrolysis mass spectra recorded at the peaks present in the TIC curve are shown. Again, the low temperature peak around 110^{o}C was due to evolution of solvent. The high temperature peaks showed maxima were at 415^{o}C and 484^{o}C indicating a significant increase in thermal stability compared to the copolymer. The relative intensities and the assignments made for the intense and/or characteristic peaks are collected in Table 4.4.

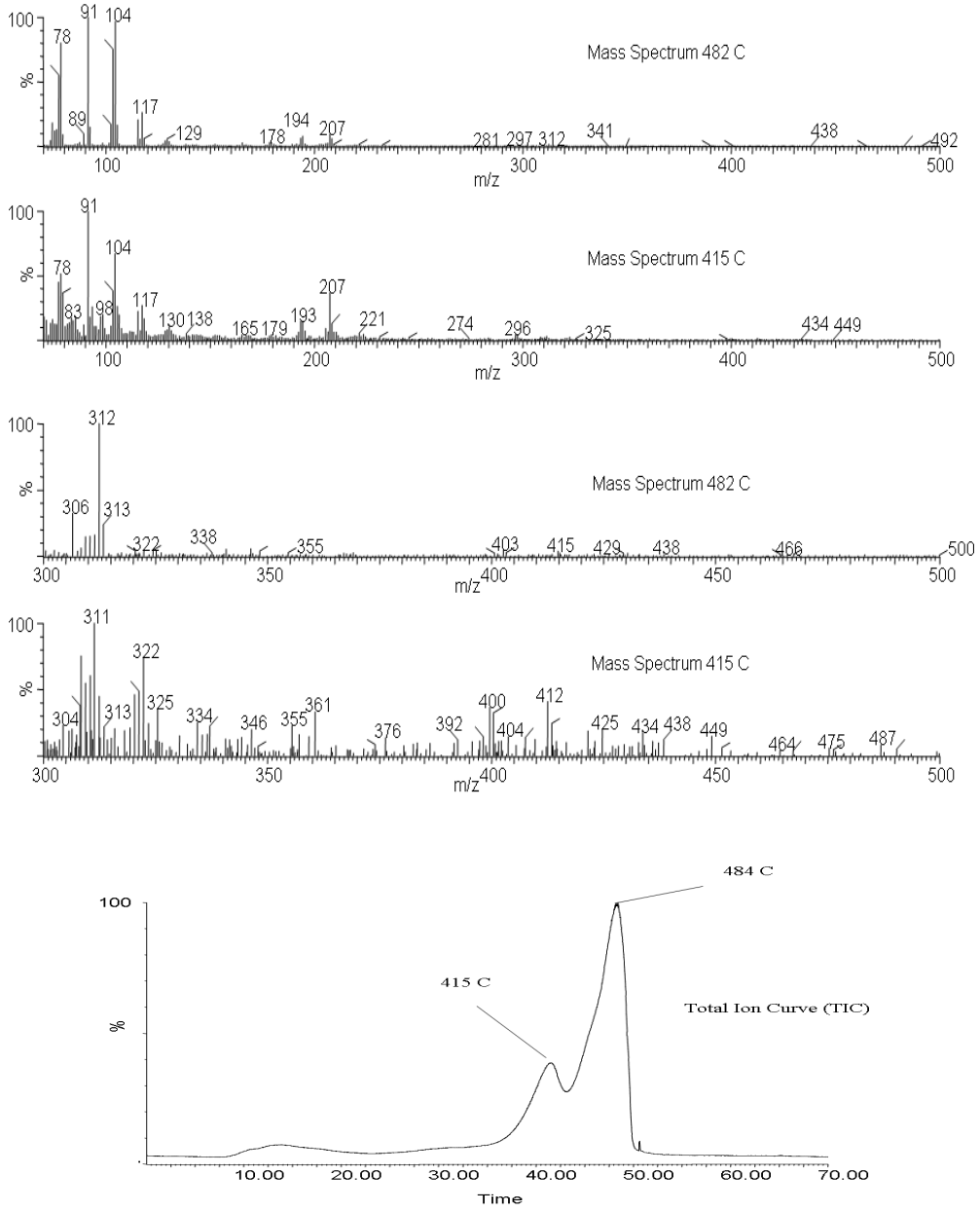

Figure 4.15. The TIC Curve and the Pyrolysis Mass Spectra Recorded at Peak Maximum and at the Shoulder for Cr-Ps-b-P2VP

Table 4.4. Relative Intensities and the Assignments for the Intense and/or Characteristic Peaks of Cr-PS-b-P2VP

m/z	408°C	414°C	482°C	491°C	Cr-PS-b-P2VP Assignment
78	988	1000	829	890	C_6H_7, C_5H_5N
91	546	750	1000	1000	C_7H_7, C_6NH_5
104	797	904	232	894	St, C_8H_8, [VP-H]
105	506	486	879	696	StH, VP
106	1000	919	116	87	VPH
117	434	428	700	474	$(C_6H_5)CH\text{-}CH{=}CH_2$, $(C_5H_4N)CHCCH_2$
118	370	323	331	253	$(C_5H_4N)CH\text{-}CH{=}CH_2$, $StCH_2$
129	30	34	552	430	$StC{\equiv}CH$
130	366	335	131	93	$PVC{\equiv}CH$, $StC{=}CH_2$
131	107	103	81	64	$StCH{=}CH_2$
132	183	165	14	11	$PVCH{=}CH_2$, $HStCH{=}CH_2$
165	31	38	160	125	$C_{13}H_{10}$,
194	160	152	506	355	$[St_2 - CH_2]$
207	492	481	645	524	$[St_2 - H]$
208	210	201	329	220	St_2 dimer, $C_{16}H_{16}$
210	28	184	10	7	VP_2 dimer
211	156	149	5.7	4.7	VP_2H
221	262	233	97	69	$St(C_6H_5)CH\text{-}CH{=}CH_2$
223	371	309	6.9	4.4	$VP_2(CH)$ St_2CH_3
233	30	27	28	18	$St_2C{\equiv}CH$
235	23	23	5.9	5.8	$PV_2C{\equiv}CH$, $St_2CH{=}CH_2$
267	3.6	3.5	2.4	2.3	$C_{21}H_{15}$
281	9	10	3.7	6.8	$C_{22}H_{17}$
298	11	14	14	14	$[St_3 - CH_2]$
306	3.2	3.8	37	36	$C_{24}H_{18}$
312	18	18	80	1.8	St_3 trimer, $C_{24}H_{24}$
315	12	14	1.1	3.0	VP_3 trimer
316	51	48	1.6	2.3	VP_3H
328	61	52	1.2	1.4	$VP_2(C_5H_4N)CH\text{-}CH{=}CH_2$
355	1.3	1.3	1.7	0.2	$VP_3C_3H_4$, $C_{27}H_{31}$
401	1.1	1.3	5.2	5.4	$[St_4 - CH]$, $C_{31}H_{29}$
429	3.5	3.1	2.3	2.4	$C_{33}H_{33}$
496	0.1	0.1	0.2	0.2	$C_{38}H_{40}$
506	0.4	0.1	0.3	0.0	$C_{39}H_{38}$

The changes in the appearance of the TIC curve with multiple peaks were quite significant. In general, the presence of more than one peak in the TIC curve and/or in the evolution profiles indicates the presence of units with different thermal stabilities. In general, the yields of products gradually decreased as the mass of the fragment increased. However, significant changes in the relative intensities of the product peaks compared to the copolymer were recorded. The relative intensities of P2VP dimer peak decreased about three folds. In Figure 4.16 single ion evolution profiles of some selected characteristic products are shown.

The products can be grouped considering the similarities in their evolution profiles. P2VP based products such as monomer (m/z=105), dimer (m/z=210), trimer (m/z=315) and tetramer (m/z=420) showed two peaks in their single ion pyrograms with maxima at around 408 and 483°C, the first being more intense and the second being quite weak. The protonated oligomers of P2VP, mainly due to H-transfer to N atom in the pyridine ring, reached maximum yield at slightly higher temperatures as in the case of pure copolymer at around 414°C. The high temperature peak was almost absent in the single ion pyrograms of the protonated oligomers. Series of products VP_xCH, VP_xC_2H and $VP_xC_2H_3$ also showed similar evolution profiles indicating random cleavages along the main chain and loss of pyridine units.

Two peaks were also present in the single ion evolution profiles of PS based products with maxima at around 414 and 483°C, but, now, the second peak was more intense. Furthermore, a shoulder around 458°C was present. Again, series of products such as St_x, St_xCH, St_xC_2H and $St_xC_2H_3$ showed similar trends in their evolution profiles. In general, for both components, the products generated by random cleavages of main chain were more intense. The peaks due to products generated by loss of C_5H_4N groups were more intense than the corresponding ones due to loss of C_6H_5 groups.

Most of these products were also detected during the pyrolysis of the pure copolymer, however, it is clear that significant changes both in the trends observed

in the evolution profiles and in the relative yields have occured. In the case of the copolymer, VP oligomers and protoned oligomers reached maximum yields at around 411 and 418°C respectively, whereas, PS based products maximized at around 428°C. For Cr-functional copolymer, in general, the relative intensities of oligomers decreased, and almost all products showed two peaks in their evolution profiles. For both components the low temperature peak with maximum at around 408-415°C may be attributed to decomposition of units retaining the thermal characteristics of the starting copolymer. However, presence of high temperature peak with maximum at 483°C in the evolution profiles of both components indicated existance of chains having significantly higher thermal stability. Another point that should be noticed was the relative yields of these peaks. For P2VP based products the low temperature peak was significantly more intense, whereas for PS based products an opposite trend was observed, the high temperature peak was noticeably more intense. These observations indicated that the presence of Cr metal affected thermal stability of both components of the copolymer.

Two set of products with m/z values 306, 401, 506 etc and 281, 355, 429, 496 etc also showed similar evolution profiles at high temperatures. These peaks were either totally absent or very weak in the pyrolysis mass spectra of the copolymer and the corresponding products showed identical evolution profiles with other PS or P2VP based products. Thus, it can be concluded that these products were mainly generated in the presence of Cr. Among these, the products with m/z values 306, 401 and 506 showed a single peak with maximum at 487°C . The others with m/z values 281, 355, 429 and 496 showed two maxima at 418 and 491°C (Fig. 4.16).

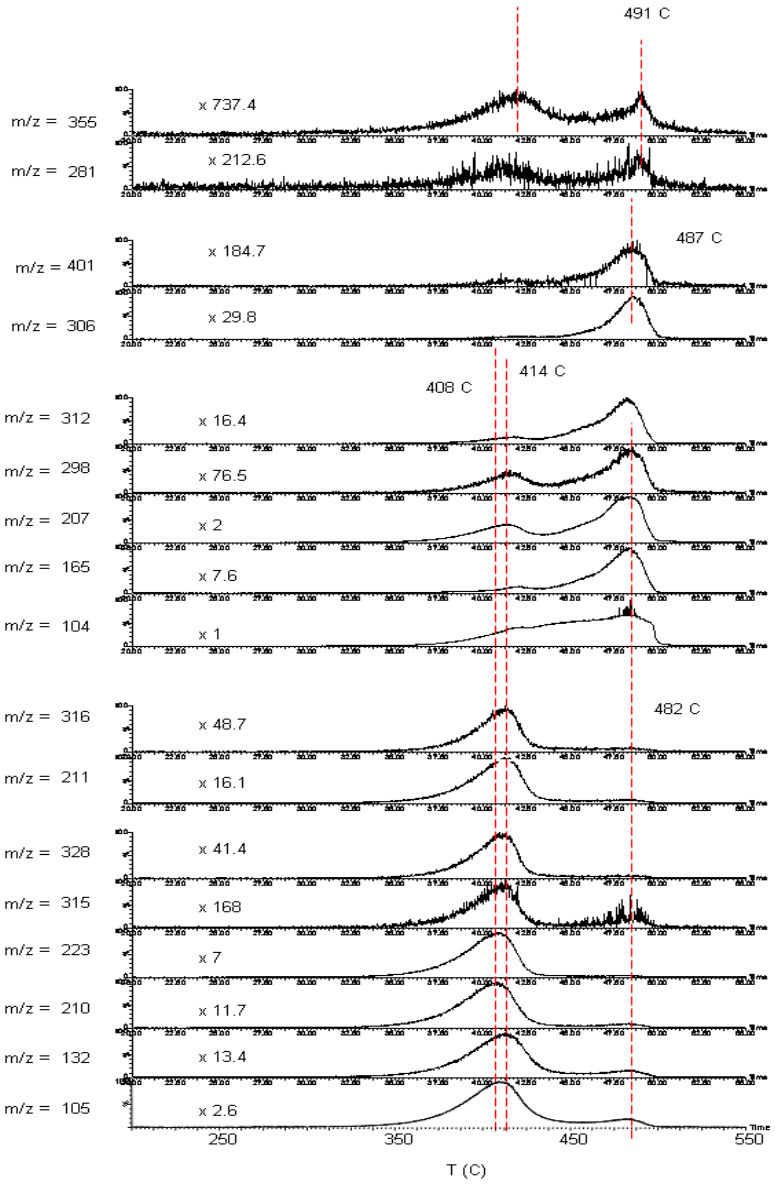

Figure 4.16. Single Ion Evolution Profiles of Some Selected Characteristic Products of Cr-PS-b-P2VP

It may be thought that due to the strong interaction between the nitrogen atom on pyridine rings of P2VP and metal, depolymerization reactions should be inhibited. Under these conditions, (C_5H_4N)-$CHCH_2$ bond can be decomposed more readily by abstracting a proton from CH_2 group leaving two adjacent radicals along the main chain. Then, either conjugated double bonds or a crosslinked structure due to intermolecular coupling reactions between the main chains of P2VP can take place as shown in Scheme 4.1.

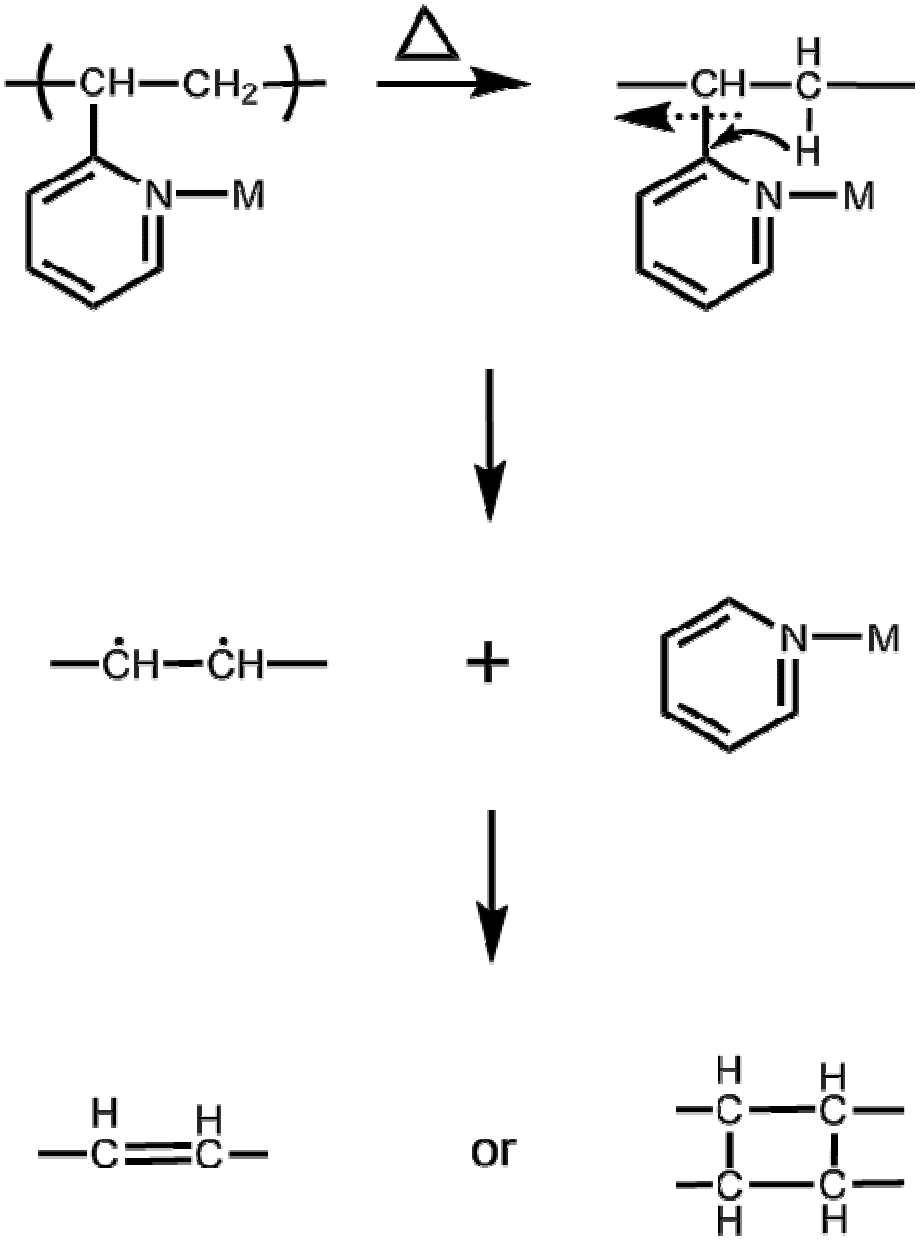

Scheme 4.1. Thermal Decomposition of Metal-Functional P2VP Chains

Decomposition of a conjugated double bonded system would yield series of $(C_2H_2)_x$ fragments and products involving H deficiency at high temperatures in accordance with present results. Then, contributions of $(C_2H_2)_x$ fragments (generated by the degradation of conjugated or crosslinked structures formed after the cleavage of metal-pyridine units) to some of the characteristic peaks of PS based products can be expected. Thus, it can be concluded that thermal decomposition of units involving metal-pyridine coordination through nitrogen occurred through the reaction pathways given in Scheme 4.1, explaining the significant decrease in the yield of P2VP based products. It can further be concluded that, the high temperature evolutions detected in the evolution profiles of PS based products were mainly due to the decomposition of conjugated or crosslinked structures generated at early stages.

4.4.3 Cobaltpolystyrene-block-poly(2-vinylpyridine)

In Figure 4.17, the TIC curve and the pyrolysis mass spectra at the peak maximum, at 464^{o}C and at the shoulder, at 412^{o}C recorded during the pyrolysis of Co-functional copolymer are shown [37]. Again evolution of solvent was detected around 110^{o}C. The evolution of thermal degradation products shifted to high temperatures compared to the copolymer indicated a significant increase in thermal stability. The relative intensities and the assignments made for the intense and/or characteristic peaks are collected in Table 4.5. Pyrolysis mass spectra recorded around 464^{o}C showed significant changes in the oligomer peak intensities. But, the more important point was the presence of peaks that were absent or very weak in the pyrolysis mass spectra of PS-b-P2VP.

In Figure 4.18 single ion evolution profiles of some selected characteristic products are shown. As can be noticed from the figure, the trends observed in the evolution profiles and relative intensities of both P2VP and PS of the copolymer based products changed significantly.

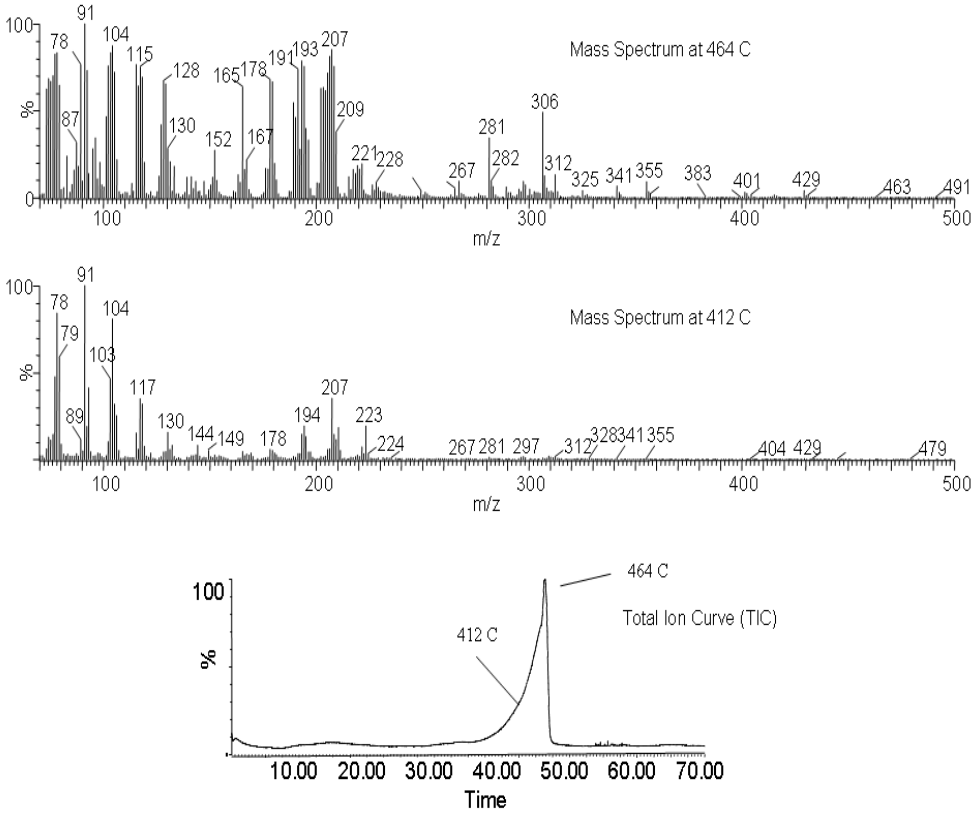

Figure 4.17. The TIC Curve and the Pyrolysis Mass Spectra Recorded at Peak Maximum and at the Shoulder for Co-PS-b-P2VP

Table 4.5. Relative Intensities and the Assignments for the Intense and Characteristic Peaks of Co-PS-b-P2VP

m/z	417°C	464°C	Co-PS-b-P2VP Assingment
91	978	1000	C_7H_7, C_6NH_5
92	186	725	C_7H_8, C_6NH_6
104	809	858	St, C_8H_8, [VP-H]
105	302	708	StH, VP
106	251	217	VPH
117	343	751	$(C_6H_5)CH\text{-}CH{=}CH_2$, $(C_5H_4N)CH{=}C{=}CH_2$
128	41	668	$StC{\equiv}C$
132	81	37	$PVCH{=}CH_2$, $HStCH{=}CH_2$
165	47	635	$C_{13}H_{10}$,
193	138	790	[St_2 – CH]
207	334	890	[St_2 – H]
208	136	750	St dimer
210	180	55	VP dimer
211	43	21	VP_2H
223	184	20	$VP_2(CH)$ St_2CH_3
267	4	87	$C_{21}H_{15}$
281	11	326	$C_{22}H_{17}$
298	7.1	72	[St_3 – CH_2], $C_{23}H_{21}$
306	8.7	490	$C_{24}H_{18}$
312	10	122	St trimer
315	4	3	VP trimer
316	6	3	VP_3H
328	5	7	$VP_2(C_6H_5)CH\text{-}CH{=}CH_2$
355	2.5	88	$C_{27}H_{31}$
401	1	33	$C_{31}H_{29}$, [St_4 – CH]
416	1	8	St tetramer
429	1	39	$St_3(C_6H_5)CH\text{-}CH{=}CH_2$, $C_{33}H_{33}$
506	0	5.5	$C_{39}H_{38}$
613	0	4.8	$C_{41}H_{44}$

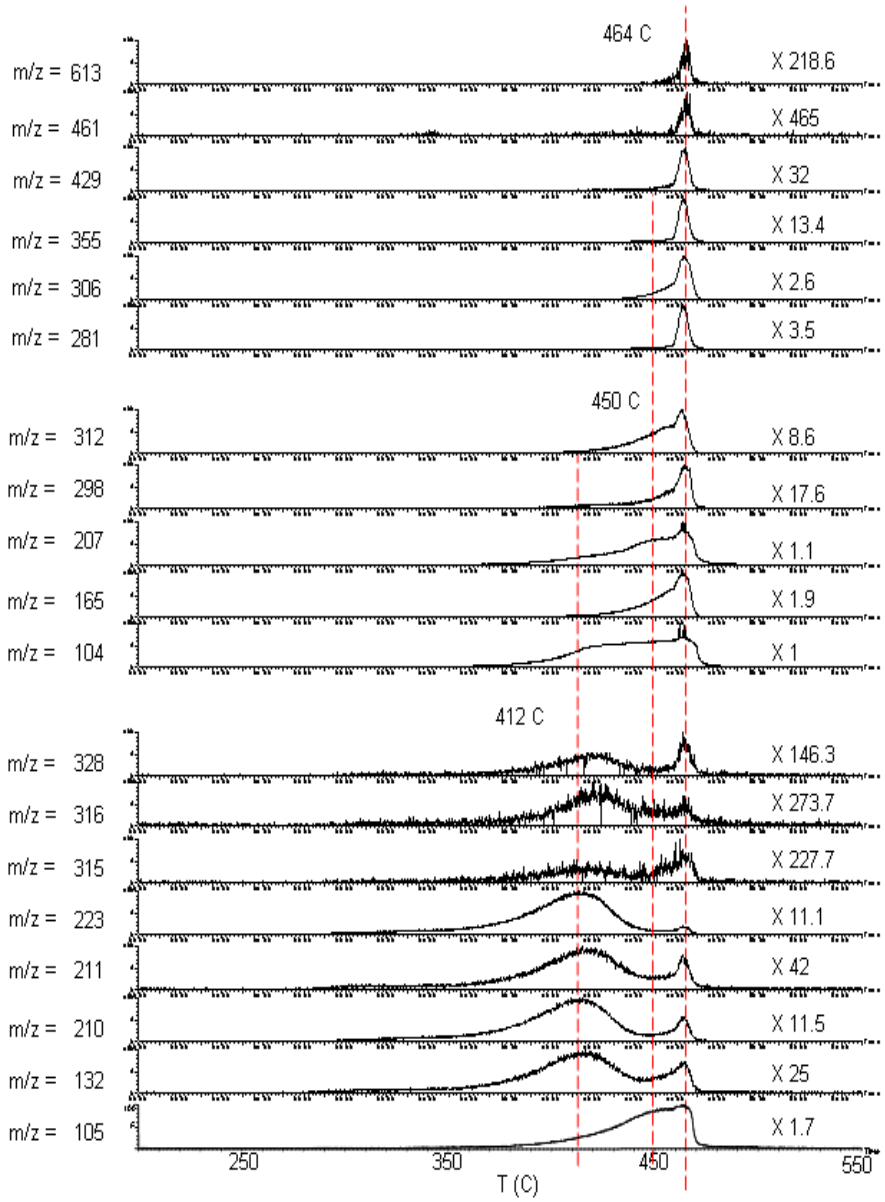

Figure 4.18. Single Ion Evolution Profiles of Some Selected Characteristic Products of Co-PS-b-P2VP

Evolution profiles of P2VP based products were sharpened and shifted slightly to high temperatures. The relative intensities of both oligomer and protonated oligomer peaks were decreased. The decrease was more significant for the protonated oligomers. Furthermore, a high temperature peak appeared in the single ion evolution profiles of P2VP based products. The two peak maxima were at 412^{o}C and 464^{o}C indicating that the increase in thermal stability was lower than that was observed for Cr functional copolymer.

The trends observed in the evolution profiles of both P2VP and PS based products indicated presence of new interactions affecting the thermal stability. The two distinct decomposition ranges observed for P2VP block can directly be associated with presence of P2VP chains with noticeably different thermal stabilities. The changes in the relative yields of the products, especially the great diminish in the protonated oligomer yields, indicated that thermal decomposition mechanism has been changed; the proton transfer to nitrogen atom was inhibited. These findings confirmed the coordination of nitrogen atom of the pyridine ring to the metal, Co. However, detection of P2VP based products around 412ºC, in the range P2VP decomposition was observed for the PS-b-P2VP pointed out the presence of unreacted vinyl pyridine units.

Significant shifts of evolution profiles of PS based products to high temperatures were also noted. Inspection of single ion evolution profiles of PS based products indicated again an increase in thermal stability. Furthermore, almost all products showed a sharp peak around 464ºC in their evolution profiles. Yet, PS based products were also generated at lower temperatures and showed either a peak or a shoulder at lower temperatures around 450ºC. However, products with m/z values 267, 281, 306, 325, 355, 429, 461, 613 showed only a single and sharp peak with a maximum at 464ºC. Thus, it can be concluded that again, as in the case of Cr – functional copolymer, the sharp high temperature peaks present in the evolution profiles of P2VP and PS based products were mainly due to the decomposition of the chains involving conjugated double bonds and/or crosslinked structure

generated along the P2VP backbone upon cleavage of pyridine units coordinated to metal.

The products that can readily be attributed to decomposition of chains involving conjugated double bonds and/or crosslinked structure occurred in a narrow temperature range around 464ºC, lower than the corresponding temperature range (480-490ºC) recorded during the pyrolysis of Cr- functional copolymer, indicating again an increase in thermal stability compared that of the copolymer but this increase was less than that was observed for the Cr analogue.

4.4.4 Goldpolystyrene-block-poly(2-vinylpyridine)

Pyrolysis mass spectrometry analysis of Au-polystyrene-block-poly(2-vinylpyridine) yielded a TIC curve showing a relatively sharp peak with a maximum at 494^{o}C and weak peaks at around 110, 230 and 383^{o}C. Again, the 110^{o}C peak was associated with evolution of the solvent. On the other hand strong HCl evolution was observed around 230^{o}C. Products due to the thermal decomposition of copolymer were recorded around 383 and 494^{o}C. In Figure 4.18, the TIC curve and the pyrolysis mass spectra recorded at 383 and 494^{o}C are shown. Detection of thermal degradation products at relatively high temperatures indicated again a significant increase in thermal stability. The relative intensities and the assignments made for the intense and/or characteristic peaks are collected in Table 4.6.

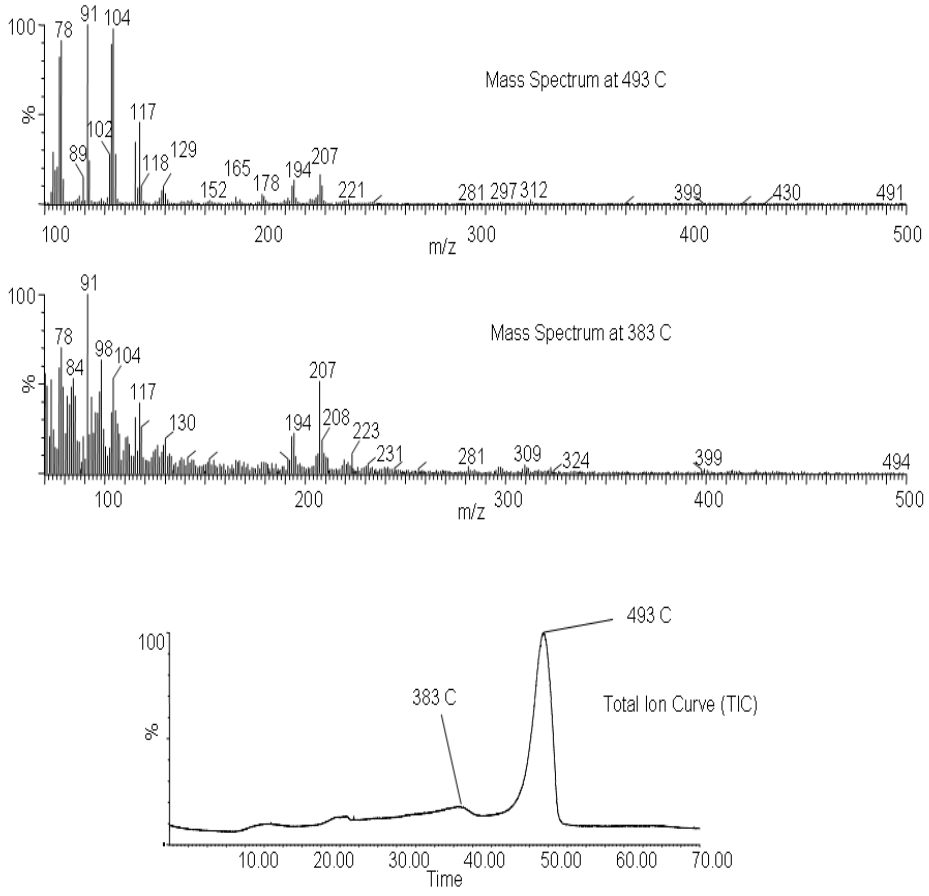

Figure 4.19. The TIC Curve and the Pyrolysis Mass Spectra Recorded at Peak Maximum and at the Shoulder for Au-Ps-b-P2VP

Table 4.6. Relative Intensities and the Assignments for the Intense and Characteristic Peaks of Co-PS-b-P2VP

m/z	390°C	494°C	512°C	Au-PS-b-P2VP Assignment
91	52	1000	1000	C_7H_7, C_6NH_5
92	8.6	238	140	C_7H_8, C_6NH_6
104	29	974	845	St, C_8H_8, [VP-H]
105	16	275	170	StH, VP
106	15	25	25	VPH
117	19	449	258	$(C_6H_5)CH\text{-}CH{=}CH_2$, $(C_5H_4N)CH{=}C{=}CH_2$
130	7.6	60	214	$PVC{\equiv}CH$
132	4	3.6	9	$PVCH{=}CH_2$, $HStCH{=}CH_2$
133	2.2	1.8	59	$HPVCH{=}CH_2$
165	4.7	36	29	$C_{13}H_{10}$, $(C_6H_5)CH{=}C{=}CH\text{-}C{=}CH\text{-}C{=}CH$
207	30	161	613	[St_2 – H]
208	8.6	95	155	St dimer
210	5.1	2.5	15	VP dimer
211	2.7	1.3	5	VP_2H
220	1.7	14	10	$St(C_6H_5)CH{=}C{=}CH_2$
221	0.4	18	20	$St(C_6H_5)CH\text{-}CH{=}CH_2$, $VP(C_6H_5)CH{=}C{=}CH_2$
222	1.9	4.2	5.9	$(VP)_x(C_6H_5)CH\text{-}CH{=}CH_2$, St_2CH_2
223	5	1.5	3.7	$VP_2(CH)$ St_2CH_3
267	0.4	0.8	11.1	$C_{21}H_{15}$
281	1.4	0.9	73.8	$C_{23}H_{19}$
306	0.6	8.6	7.4	$(C_6H_5)CH{=}CH\text{-}CH{=}CH\text{-}CH{=}CH\text{-}C{\equiv}C\text{-}CH{=}CH_2$
312	0.6	20	3.7	St trimer
315	0.5	0.1	0.4	VP trimer
316	0	0.3	0.0	VP_3H
328	0.3	0.4	2.2	$VP_2(C_6H_5)CH\text{-}CH{=}CH_2$
355	0	0.3	9.6	$C_{27}H_{31}$
401	0.4	1	3.3	$C_{31}H_{29}$, [St_4 – CH]
429	0.4	0.2	9.2	$St_3(C_6H_5)CH\text{-}CH{=}CH_2$, $C_{33}H_{33}$
432	0.1	0	2.2	$VP_3(C_6H_5)CH{=}C{=}CH_2$
461	0	0	0.4	$C_{36}H_{29}$
506	0.1	0.3	1.1	$C_{39}H_{38}$

No other product peak was observed in the region where HCl evolution was detected pointing out that, the evolution of HCl had no significant effect on thermal stability of the copolymer. In general, for this sample, thermal decomposition mainly took place around 494^{o}C and the product yield was quite low below 450^{o}C. In Figure 4.20, single ion evolution profiles of some selected characteristic products are shown.

Similar P2VP based thermal degradation products were also detected for Au-PS-b-P2VP. It can be observed both from Table 4.6 and from the evolution profiles that the relative intensities of P2VP based products decreased drastically, more than what were observed for Cr and Co functional copolymers. Two peak maxima were recorded in the evolution profiles of all products, except for the protonated oligomers, at 390^{o}C and 494^{o}C. The protonated oligomers showed a single peak around 390^{o}C in their evolution profiles, the maximum yield was detected at slightly higher temperatures as in the case of pure copolymer at around 414^{o}C. Although detection of P2VP based products around 390^{o}C, in the temperature range where P2VP decomposition was observed in the case of pure copolymer, pointed out the presence of unreacted vinyl pyridine units. However, the drastic decrease in the relative intensities of P2VP based products indicated that the extent of uncoordinated pyridine units was quite low.

Unlike P2VP based products, PS based products were significantly intense. Evolution profiles of PS based products shifted to higher temperatures showing an intense and broad peak with a maximum at 494^{o}C (Fig. 4.20). This shift was much greater than that were detected for Cr and Co analogues. In the evolution profiles of [St_2 – H] at m/z=207 a sharp peak with a maximum at 512^{o}C was also detected.

All products associated with the thermal degradation of chains involving conjugated double bonds and/or crosslinked structure generated along the P2VP backbone upon cleavage of pyridine units coordinated to metal, such as products with m/z values 281, 325, 355, 401 and 429 evolved in narrow temperature range and their yields were maximized at 512^{o}C similar to the high temperature peak in

evolution profile of styrene dimer. Thus, it can be concluded that the high temperature peak in the evolution profile of product with m/z value of 207 was mainly due to $C_{16}H_{15}$ fragment generated during the decomposition of chains having conjugated double bonds and/or crosslinked structure.

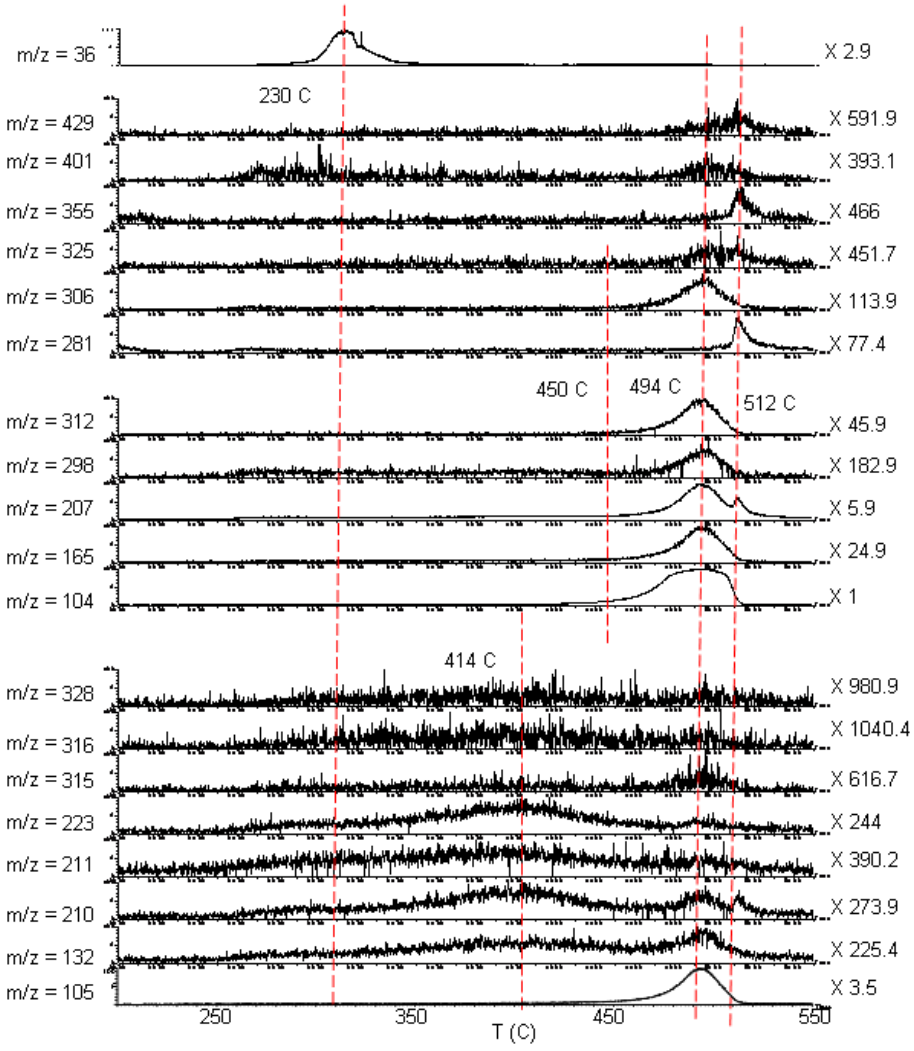

Figure 4.20. Single Ion Evolution Profiles of Some Selected Characteristic Products of Au-PS-b-P2VP

CHAPTER 5

CONCLUSIONS

In this study, metal functional polymers, namely Cr-PS-b-P2VP, Co-PS-b-P2VP, Au-PS-b-P2VP, Fe-PS-b-P2VP and Mo-PS-b-P2VP were synthesised by thermal reactions of hexacarbonylchromium, $Cr(CO)_6$, octacarbonyldicobalt $Co_2(CO)_8$ hydrogenotetrachloroaurate(III), $H(AuCl_4).4H_2O$,trichloroiron(III), $FeCl_3.6H_2O$, molybdenum(VI)oxide, MoO_3, and PS-b-P2VP. TEM images indicated nanoparticle formation as a result of the reactions of PS-b-P2VP with the Au^{III}, Cr and Co. On the other hand, crystalline structures were detected for Fe-PS-b-P2VP and Mo-PS-b-P2VP. Samples involving nanoparticles were further characterized by FTIR, UV-Vis and pyrolysis mass spectrometry techniques. Results of the study can be summarized as:

- TEM images of metal nanoparticles showed that the size of Cr and Co nanoparticles are between 10-20 nm, however, Au nanoparticles are smaller than 10 nm.

- FTIR analysis indicated dissapearance of characteristic carbonyl peaks of $Cr(CO)_6$ and $Co_2(CO)_8$ for Cr-PS-b-P2VP, Co-PS-b-P2VP samples. Decreases in the intensities of the diagnostic peaks due to C-H stretching and bending modes and C-C and C=C stretching modes of pyridine ring were observed for all Cr-PS-b-P2VP, Co-PS-b-P2VP and Au-PS-b-P2VP samples. Furthermore, the appearance of a peak at about 467 cm^{-1} supported metal bonding to nitrogen.

- The results of pyrolysis mass spectrometry analysis can be summarized as ;
    - No change in the thermal stability of P2VP chains involving uncoordinated pyridine units.
    - Thermal degradation mechanism of P2VP chains coordinated to metals or metal ion through pyridine units were changed significantly; the cleavage of pyridine units coordinated to metal or metal ion, generation of conjugated unsaturated and/or crosslinked polymer backbone and degradation of this thermally more stable chains at high temperatures.
    - Thermal stability of these chains increased depending on the type of the metal or metal ion present in the order Co< Cr <Au^{3+} indicating a stronger interaction between the metal or metal ion with nitrogen atom on pyridine.

REFERENCES

[1] Bochman, M., *Organometallics 1 Complexes with Transition Metal-Carbon σ-Bonds*, New York, 1994.

[2] Williams K.A., Boydston A.J., Bielawski C.W., *Chemical Society Reviews,* 2007, 729

[3] Pesetskii, S.S., Jurkowski, B., Krivoguz, Y.M., Davydov, A.A., Bogdanovich, S.P. *Journal of Applied Polymer Science,* 2007, 1366.

[4] Lazzari, M., Arturo Lopez-Quintela, M., *Advanced Materials*, 2003, 1583-1584.

[5] Chen, Z., Kornfield, J.A., Smith. S.D., Grothaus, J.T., Satkowski, M.M., *Science,* 1997, 277, 1248-1249.

[6] Grubbs, R.B., *Highlight,* 2005, 4324-4325.

[7] Hacaloğlu, J., Fares, M.M., Süzer, Ş., *European Polymer Journal*, 1997, 939.

[8] Fares, M.M., Yalçın, T., Hacaloğlu, J., Güngör, A., Süzer, Ş., *Analyst*, 1994, 693.

[9] Qian, K., Killinger, W.E., Casey, M., Rapid polymer identification by in-source direct pyrolysis mass spectrometry and library searching techniques, *Anal. Chem*., 1996, 68, 1019-1027.

[10] Blazso, M., Recent trends in analytical and applied pyrolysis of polymers, *J. Anal. Appl. Pyrolysis*., 1997, 39, 1-25.

[11] Tsuge, S., Ohtani, H., Structural characterization of polymeric materials by pyrolysis GC/MS, *Polym. Deg Stab*., 1997, 58, 109-130.

[12] Parsi, Z., Górecki, T., Poerschmann, J., Advances in non-discriminating pyrolysis, *J. Anal. App. Pyrolysis*, 2005, 74, 11-18.

[13] Wapler, T.P., Practical applications of analytical pyrolysis, *J. Anal. Appl. Pyrolysis*, 2004, 71, 1-12.

[14] Lattimer R.P., Pyrolysis field ionization mass spectrometry of hydrocarbon polymers, *J. Anal. Appl. Pyrolysis*, 1997, 39, 115-127.

[15] Suvanto, S., Pakanen, T.A., Backman, L., *Applied Catalysts*, 1999, 177, 25-36.

[16] Rutnakornpituk, M., Thompson, M.S., Harris, L.A., Farmer, K.E., Esker, A.R., Riffle, J.S., Conolly, J., St. Pierre, T.G., *Polymer*, 2002, 43, 2337-2348.

[17] Aizawa, M., Buriak, J.M., *J.Am.Chem.Soc*., 2007, 128, 5879.

[18] Diana, F.S., Lee, S., Petroff, P.M., Kramer, E.J., *Nano Letters*, 2003, 3, 892.

[19] Shriver, D. F., Atkins, P.W., Langford, C.H., *Inorganic Chemistry*, John Willey & Sons, Inc., Oxford,1990.

[20] Cotton, F.A., Wilkinson, G., *Advanced Inorganic Chemistry*, John Willey & Sons, Inc., New York, 1972.

[21] Huhey, J.E., *Inorganic Chemistry*, Harper & Row, New York, 1983.

[22] Baranauskas, V.V., Zalich, M.A., Saunders, M., St, Pierre, T.G., Riffle, J.S., *Chem. Mater.*, 2005, 17, 5246-5254.

[23] Mason, W.R., Gray, H.B., *Inorg. Chem.*, 1968, 7, 55.

[24] Mason, W.R., Gray, H.B., Gray. *J. Am. Chem. Soc.*, 1968, 90, 5721.

[25] Isci, H., Mason, W.R., *Inorg. Chem.***,**1983, 22, 2266.

[26] Schmidtke, H.H., Garthoff, D., *J. Am. Chem. Soc.*, 1967, 89, 1317.

[27] Paw, W., Cummings, S.D., Mansour, M.A., Connick, W.B., Geiger, D.K., Eisenberg, R., *Coord. Chem. Rev.***,** 1998, 171, 125.

[28] Hess, P., Parker, P.J., *Appl. Polym. Sci.*, 1966, 10 (12), 1915.

[29] Sastri, S.B., Armistead, J.P., Keller, T.M., Sorathia, U., *Polym. Compos.*, 1997, 18, 48.

[30] Sastri, S.B., Keller, T.M., *J. Appl. Polym. Sci.*, 1998, 36, 1885

[31] Sastri, S.B., Keller, T.M., *J. Appl. Polym. Sci.*, 1998, 36, 1885

[32] Sumner, M.J., Sankarapandian, M., McGrath, J.E., Riffle, J.S., *Polymer*, 2002, 43, 5069.

[33] Sumner, M.J., Sankarapandian, M., McGrath, J.E., Riffle, J.S., Sorathia, U., *International SAMPE Technical Conference*, SAMPE, Covina, CA, 2001, 33, 1509.

[34] Tannenbaum, R., *Inorg. Chim. Acta*, 1997, 227, 233.

[35] Nogues, J., Schuller, I.K., *J. Magn. Magn. Mater.*, 1999, 192, 203.

[36] Connolly, J., St. Pierre, T.G., Rutnakornpituk, M., Riffle, J.S., *Eur. Cells Mater.*, 2002, 3, 106.

[37] A.G., Elmacı, "Thermal Characterization of Homopolymers, Copolymers and Metal Functional Copolymers of Vinylpyridines", Middle East Technical University, Graduate School of Natural and Applied Science, Department of Chemistry, 2008. (In Preparation)

[38] Howell, B.A., Ther, J., *Anal. Cal.*, 2007, 89, 393.

[39] McNeill, I.C., *Angew Makromol Chem*., 1997, 247, 179.

[40] Kannan, P., Biernacki, J.J., Visco, D.P., *J. Anal Appl. Pyrolysis*, 2007, 78, 162.

[41] Poutsma, M.L., *Polym. Deg. Stab.*, 2006, 91, 2979.